Dynamical systems, numerical experiments and super-computing

Carles Simó

Departament de Matemàtica Aplicada i Anàlisi, Universitat de Barcelona,
Gran Via, 585, 08071 Barcelona (Spain)
E-mail: carles@maia.ub.es

Abstract

Dynamical systems study the evolution models of natural phenomena and the simplified models which help to understand them. They can be given in deterministic form, either by means of ordinary differential equations, partial differential equations or discrete maps. They are useful in all domains of science and technology.

In their study tools from all areas of mathematics are used. But for systems with some degree of complexity it is impossible to produce a fairly complete description of the evolution in the space of states, and its dependence with respect to parameters, without using numerical techniques. They are essential for concrete applications and very useful even for theoretical studies. They can be seen as an experimental part of mathematics.

In the last years it has become possible to achieve a generalisation in the systematic use of numerical experiments, due to the availability of large arrays of processors working in parallel with a reduced cost. But the impact of new algorithms has been even larger. This makes feasible to face problems of larger and larger complexity.

In this lecture some aspects of the general methodology and several examples are presented.

Resum

Els sistemes dinàmics estudien els models d'evolució de fenomens naturals, i els models simplificats que ajuden a entendre'ls. Poden estar donats de forma determinista, sigui mitjançant equacions diferencials ordinàries, en derivades parcials o transformacions discretes. Són útils en tots els camps de la ciència i la tècnica.

En el seu estudi s'empren eines de tots els dominis de la matemàtica. Però per a sistemes d'un cert grau de complexitat no hom pot fer una descripció mínimament completa de l'evolució a l'espai d'estats i la seva dependència respecte paràmetres sense recòrrer a tècniques numèriques. Són essencials per les aplicacions concretes i útils encara que l'objectiu sigui l'estudi teòric. Es pot mirar això com una part experimental de la matemàtica.

En els darrers anys ha estat possible un grau de generalitat considerable en l'ús sistemàtic de l'experimentació numèrica degut a la disponibilitat de gran quantitat de processadors treballant en paral·lel i de forma econòmica. Però l'impacte de nous algorismes ha estat encara superior. Això fa que siguin abordables problemes de notable dificultat.

En l'exposició es detallen la metodologia general i alguns exemples concrets.

Contents

1 Introduction

To study the dynamics of a system in evolution one has to consider a mathematical model which tells us how this evolution takes place. One of the most common models are the ordinary differential equations (ODE)

$$x' = \frac{dx}{dt} = f(t, x, \mu), \tag{1}$$

where t denotes time and x the set of variables in evolution. The μ denote parameters which can appear in the equation. Higher order equations (e.g., the equations of the mechanics) can always be written as a system of first order equations. We consider the x in (1) belonging to some open set in $\mathbb{R}^n$ or to a manifold.

In case we want to study the evolution of a magnitude $u = u(t, x)$ depending on time and space, we are faced to partial differential equations (PDE) of evolution type

$$\frac{\partial u}{\partial t} = F(t, x, u, \frac{\partial u}{\partial x}, \frac{\partial^2 u}{\partial x^2}, \ldots). \tag{2}$$

Assume x belongs to some domain Ω. These PDE can be put again in the form (1) by considering a function v defined in Ω and that this function depends on time, so that $u(t,x) = (v(t))(x)$. The setting is similar to the ODE case, but now we look for a $v(t)$ which belongs to a functional space. To make numerical simulations this infinite dimensional functional space is approximated by a finite dimensional one, so that we fall again in case (1).

Other models are discrete and they give information on how a variable changes at each step

$$x \mapsto T(x). \tag{3}$$

Typically it is assumed that T is a diffeomorphism, that is, a map which is regular enough (differentiable r times or even analytic) and which is invertible. This is the case, for instance, if we consider (1) of autonomous type (i.e., independent on t) and consider T as the flow time h of (1) for a fixed value of h. There are other natural devices (e.g., the Poincaré maps or first return of the flow of (1) to a given section, under suitable conditions) to obtain discrete models.

In any case, either if we consider equations like (1) in the autonomous case or maps as (3) we have a phase space or state space, where x moves in a continuous or discrete way. In the case (1) if f is autonomous, we have an stationary vector field in each point of the state space. One can consider, as fundamental steps to "understand" the system, the following ones:

- To identify simple objects, such as fixed points and periodic orbits, or other invariant objects (i.e., left invariant by the flow or the map), such as spheres, tori, etc, in the state space.

- To study the stability of these objects. Assume they are unstable and it is possible to escape from a vicinity of them when t increases or we iterate under T repeatedly. Then we want to describe the set of points which tend to the invariant object when going backwards in time. This set is called unstable manifold. In a similar way we can study stable manifolds (if any), i.e., the sets of points tending to the invariant object in forward time.

- To look at the possible connections between unstable and stable manifolds of the same or different invariant objects. These are the so-called homoclinic and heteroclinic orbits. Under some conditions (transversality of the manifolds) they give rise to complicated dynamics, diffusion, strange attractors, etc.

  It became popular to denote this dynamical behaviour as chaos, despite a very clear explanation is found in terms of homoclinic orbits. The more relevant feature is the the lack of predictability, despite systems as (1) or (3) are deterministic.

  The invariant objects and their possible connections constitute the "skeleton" of the dynamics. They give a key tool to understand the full dynamics.

- All the previous objects and structures can depend on parameters (e.g., physical parameters of the model). Hence, it is interesting to see how stable is the behaviour when the parameters change, which kind of changes or bifurcations are possible and the different patterns of the corresponding dynamics. This is applicable, for instance, if one can act on the parameters to obtain the most desirable effects.

In what follows we shall present a few examples of dynamics and some methodology which helps to learn about them, based on numerical experiments. We shall review on how useful this approach is to carry out later the corresponding theory. This leads, in a natural way, to discuss on the role of computers on the progress in mathematics. As an additional item one has to think about the computational resources, which lead to a need known as "super-computing". Some conclusions close the presentation.

2 Invariant objects

The simplest invariant objects are fixed points. They are found by solving for

$$f(x) = 0 \qquad \text{or} \qquad T(x) - x = 0, \tag{4}$$

that is, as most of mathematics, can be formulated as an equation to be solved.

Invariance of other objects can be put in a similar way. Assume we look for an invariant closed curve γ of a diffeomorphism T, and such that the dynamics in γ is equivalent, after some change of variables, to a rotation of angle ω. Let θ be an angle in $\mathbb{S}^1$ used to parametrise γ and express the points in γ as the image of $\mathbb{S}^1$ by a function g. The invariance condition can be expressed as

$$T(g(\theta)) = g(\theta + \omega) \qquad \text{or} \qquad T(g(\theta)) - g(\theta + \omega) = 0, \tag{5}$$

again an equation like (4). Now we do not look for a point x but for a function g. This can be solved by Fourier methods.

We can also look for invariant objects as the graph of a function. Assume a fixed point in $\mathbb{R}^n$ has an unstable manifold of dimension m. After a suitable splitting of the components of x in two groups, y and z, we can look for the invariant manifold in the case of ODE as follows. Let $y = g(z)$ a function such that its graph gives the desired manifold. As it should be invariant, the derivative of $y - g(z)$ must be zero. But the derivatives of y and z are expressed in terms of the components of x, that is, in terms of y and z. Hence, we get

$$y'(g(z), z) = Dg(z)g'(g(z), z), \tag{6}$$

where Dg denotes the differential of g. Again, as in (5) we are lead to an equation for g, which can be solved by Taylor series methods. One can see [23] for relevant information and [24] for explicit illustrations on the use of the methods.

The solution of equations like (5) or (6) is typically done by symbolic manipulation: one looks for formal series expansions up to the desired order. This can be useful, for the purpose to obtain local approximations, even if the series are not convergent but they have an asymptotic character, as we shall see.

To obtain these expansions in fully analytic form, that is, carrying explicitly in a literal form the dependence with respect to parameters and initial conditions, can be cumbersome. Only low order expansions are available. It is advisable to produce semi-analytic expansions, in which some variables are kept in literal form while the coefficients are computed as number (with the desired accuracy).

Some examples illustrate the computation of invariant objects.

2.1 Capture and escape in the Sitnikov problem

In many N-body problems it is interesting to locate the regions of capture and escape: An asteroid or a comet can be captured (or captured for some time) by a planet, for instance. Systems of binary stars can capture a third star or eject it. The boundaries of capture and escape are related to invariant manifolds of suitable objects.

The Sitnikov problem provides one of the simplest examples. The problem consists of two massive bodies, of equal mass, moving on the horizontal plane and describing ellipses of eccentricity e around the centre of masses, which is assumed to be at the origin. A third particle of negligible mass and, hence, without any influence on the two massive bodies, moves on the z axis. The equations of motion, assuming the masses equal to 1/2, are

$$\ddot{z} = -\frac{z}{(z^2 + r(t)^2/4)^{3/2}}, \tag{7}$$

where $r(t)$ is the distance between the massive bodies at time t, as given by the solution of Kepler problem. If $e=0$ the massive bodies move on circular orbits, that we can assume have radius $\rho=r/2=1/2$ and period 2π, by normalising the units of distance and time. Then the motion is integrable and if the energy of the infinitesimal particle $h=\frac{1}{2}-\frac{1}{(z^2+1/4)^{1/2}}$ is below 0, the particle remains confined for all time. If $h>0$ the particle escapes, tending to infinity with finite velocity, $\dot{z}|_{t\to\infty}=(2h)^{1/2}$. In the critic case $h=0$ the particle tends to infinity with zero limit velocity. This is the so-called parabolic escape.

It is relevant to remark that in the parabolic case the two massive bodies keep moving in a circular orbit. Hence the motion still has a part which is 2π-periodic. Introducing new coordinates, as done by McGehee, see [20, 21],

$$z=2/q^2, \qquad \dot{z}=-p \tag{8}$$

and introducing a new time, the parabolic escape is seen as a fixed point $q=p=0$ and the equations are still 2π-periodic in t. This invariant object is called the "periodic orbit at infinity".

Instead of looking at the solution $z(t)$ it is simpler to look at the successive passages through $z=0$ (at least one such passage occurs). At these passages we can record the values of $t \pmod{2\pi}$ and of $|\dot{z}|$. This is enough to specify the orbit. It is clear that for $e=0$ the successive values of $|\dot{z}|$ are equal ($(4+2h)^{1/2}$) and the successive values of t are equispaced: $t_{k+1}-t_k=\text{ctant}$, a constant depending on h. The boundary capture-escape corresponds to $|\dot{z}|=2$.

If $e\neq 0$ the situation is quite different: The system is no longer (globally) integrable and the boundaries of the capture and escape regions do not coincide. In particular there are quasi-random motions. This was the purpose of Sitnikov when he introduced this example. And this serves also to illustrate the existence of oscillatory solutions, as conjectured by Chazy: orbits defined for all time with $\liminf r(t)$ finite and $\limsup r(t)=\infty$.

To compute the boundaries amounts to compute the invariant manifolds of the periodic orbit at infinity. Equations (7) are transformed to the new variables introduced in (8) and it is convenient to use as independent variable the eccentric anomaly E of the motion of the massive bodies. The invariant manifolds can be expressed as graphs of functions of the form

$$p(E,e,q)=\sum_{k\geq 1}\sum_{j\geq 0}\sum_{i\geq 0} c_{i,j,k}e^i \,\mathrm{sc}(jE)\, q^k, \tag{9}$$

where the $c_{i,j,k}$ are rational coefficients, sc denotes either the sine or the cosine functions and the coefficients are determined to have invariance, see (6). In fact, for a given k the values of i and j are bounded by k, and some parity rules must be satisfied. Furthermore the stable manifold can be obtained from the unstable one by a symmetry.

The coefficients $c_{i,j,k}$ are determined by some recurrent relations. This makes possible to obtain effectively them to high order in k. A routine computation allows to have the coefficients up to k greater than 500 (in all near 3.2 million coefficients). Not all these coefficients will be used. The purpose has a theoretical character. Defining $a_k=\sum_{j\geq 0}\sum_{i\geq 0}|c_{i,j,k}|$ as the norm of the coefficients at order k, it has been checked that $a_k \simeq (k/3)!$ This suggests, not only that $p(E,e,q)$ is not analytic in q, but that it is of Gevrey class 1/3, uniformly in (E,e) for $e\in(0,1]$. This fact has been proved theoretically in [14].

Furthermore the expansion allows to determine the optimal order $k_{\max}$ to be used, in such a way that the order of the error in the representation of the manifold is at most $\varepsilon=10^{-16}$, uniformly in (E,e), for values of q as large as possible. It has been found $k_{\max}=80$ and the representation is accurate up to ε for $q\leq q_{\max}=0.2$. Hence, for a given e we take $q=q_{\max}$ and a sample of values of E. They are inserted in (9) to evaluate p and have initial data on the unstable manifold. Then they are transformed back to $(z,\dot{z})$ variables using (8) and then (7) is integrated numerically until z reaches

0. Note that it is important to have q as large as possible, to minimise the effort of the numerical integration.

Some results are shown in Figure 1, where the (first) intersections of the unstable and stable manifolds of the periodic orbit at infinity with $z = 0$ are shown, representing them in polar coordinates: the radius is $|\dot{z}|$ and the angle is t. We note how the lack of coincidence of stable and unstable manifolds increase with e. In three plots we show $e = 0.5, 0.9, 0.999$. Last plot shows the angle of intersection of these manifolds, plotted as a function of e. The intersections occurring on the right part are shown as a function of e, while the ones on the left part are shown as a function of $-e$. Successive intersections of the manifolds (i.e., new intersections with $z = 0$ if they occur) can also be computed. Then the dynamics of the particle will be completely determined by its position with respect to these intersections. For instance, points outside the curves shown as continuous lines are not captured, while points inside are. In a similar way, points outside the curves drawn in broken lines escape, but points inside them have at least one return to $z = 0$.

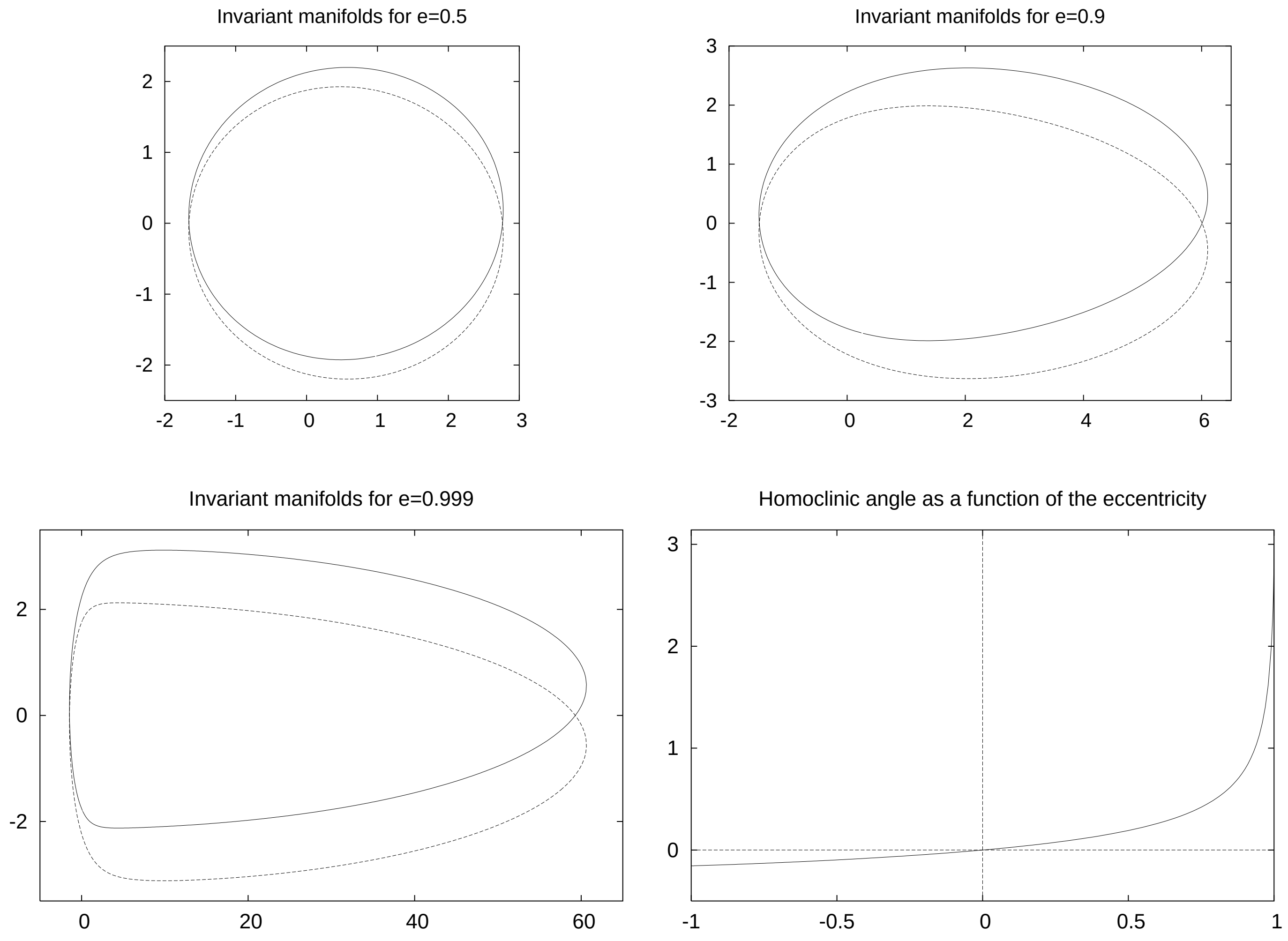

Figure 1: Boundaries of the domains of capture (plotted as continuous lines) and escape (plotted as broken lines) in Sitnikov problem for three values of e, as shown. The right bottom plot displays the angles at the intersections of these boundaries as a function of e or $-e$. See the text for additional details.

2.2 Some additional examples in Celestial Mechanics

(A) The computation of fixed points seems to be, in principle, an easy task. However the following example shows that to be able to obtain all fixed points can be a difficult problem.

Let us consider the N-body problem. It is clear from the equations of motion (with normalised masses, which is always possible)

$$\ddot{x}_j = \sum_{i=1,\dots,N,\, i\neq j} \frac{x_j - x_i}{r_{i,j}^3},\ j = 1,\dots,N, \qquad r_{i,j} = ||x_j - x_i||_2, \qquad \sum_{i=1}^{N} m_i = 1, \tag{10}$$

where $x_j \in \mathbb{R}^2$ and m_j denote position and mass of body number j, that no fixed points exist. However we can consider solutions such that are fixed in a rotating frame around the centre of masses. Then the centrifugal force will cancel the gravitational attraction. These solutions exists and are known as relative equilibrium solutions (RES). Two of them are considered equivalent if can be obtained one from the other by rotation and scaling. Let us denote also as RES(N) the number of non-equivalent RES for N bodies. If $N = 2$ they correspond to circular orbits around the centre of mass, that is RES(2)=1. If $N = 3$ there exist the well-known collinear and triangular solutions due to Euler and Lagrange, that is RES(3)=5. For $N = 4$ an exhaustive numerical exploration was done in [22] showing that 34 $\leq$RES(4)$\leq$ 50. In contrast to the 3-body problem the number RES(4) depends on the values of the masses. Therefore one has to use the notation RES($m_1, \dots, m_N$). The maximal number is attained only if the masses are equal or very close.

What happens for $N = 5$? It is simpler, first, to study limit cases. That is, assume that $N = n+m$ and we consider a problem with n massive bodies and m infinitesimal ones. It is clear that the n bodies must be in a RES. For each one of these configurations the m bodies have different possibilities, and one has to distinguish between the cases if which these bodies are at finite of infinitesimal distance. For concreteness we assume that the masses of the large bodies are equal, and the masses of the infinitesimal bodies are also all equal to μ and we consider the limit case $\mu \to 1$.

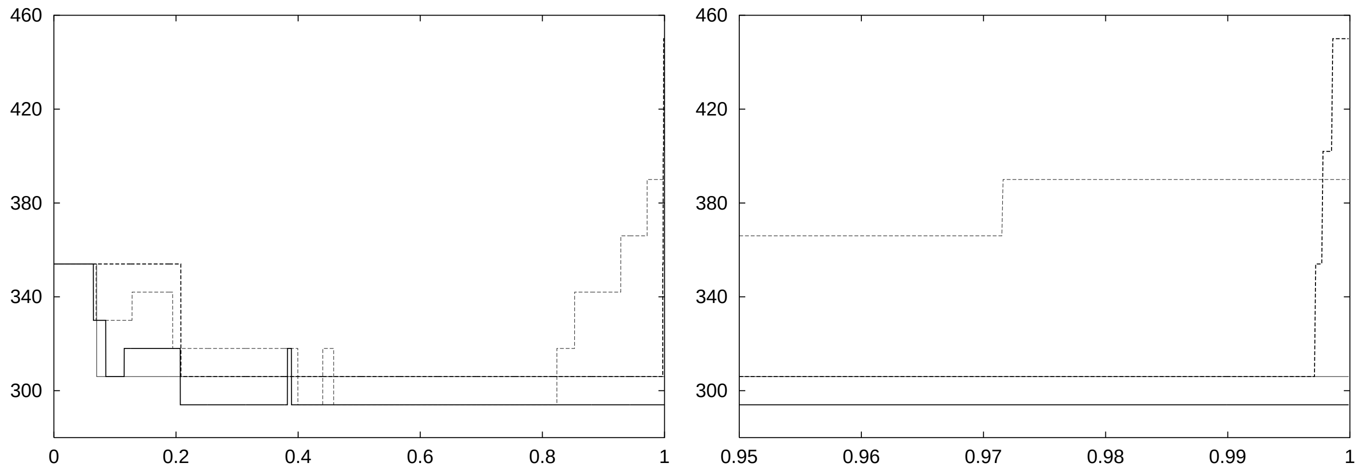

Figure 2: Left: Evolution of the number of relative equilibrium solutions in the 5-body problem when going, in the space of masses, from 5 equal masses to a limit case. The limits are: the 1+4 problem (continuous thin line); the 2+3 problem (continuous thick line); the 3+2 problem (broken thin line); the 4+1 problem (broken thick line). Right: A magnification close to the limit cases.

For $N = 5$ the possibles values of n range from 4 to 1. The following results are proved in [19]:

The 4+1, 3+2, 2+3 and 1+4 problems have 450, 390, 294 and 306 RES, respectively.

Partial results of a numerical exploration show evidence that for equal masses there are 354 RES, and that the minimum value for RES(5) is 294. In contrast with the case $N = 4$ the maximum is not achieved for equal masses. Furthermore there is another important difference: For $N = 4$ it seems that the solutions for all masses can be obtained by continuation along a suitable line, in the mass space, joining the equal mass case with a limit case (the limit case taken with arbitrary masses of the finite bodies). All solutions for all masses can be reached by continuation along such a line, starting at equal masses or at a limit case.

For $N = 5$ this seems no longer true. Figure 2 displays the number of RES found along a line which has parameter equal to 0 for equal masses and equal to 1 in the limit case. [1]

We remark that the RES give rise to the only regular solutions which can be obtained explicitly for the N-body problem (if the RES can be found by some method). Furthermore they play a relevant role in the study of the topology of the set of points of the phase space with a given energy and angular momentum.

(B) A different problem arises when we look for periodic solutions not coming from a RES. Recently, after the remarkable proof of the existence of a "figure-eight" orbit in the three-body problem [7], a large amount of work has been devoted to the study of "choreographies".

A choreography is a periodic solution of the N-body problem with equal masses, such that all bodies move along the same curve in the configuration space, having a constant time shift between one body and next one. For motivation and different results one can check [27, 6, 29].

Choreographies which can be obtained one from the other by scalings, rotations and time shift, are considered as equivalent. If a choreography has a central manifold associated to it, then the choreographies in this manifold can be seen as "satellite choreographies" of the initial one, see [27]. One can also consider orbits which become choreographies in some rotating frame, or relative choreographies, see [29].

One of the standing problems is if there are infinitely many non-equivalent choreographies, letting aside satellite and relative ones. The numerical results in [29], where several hundreds of choreographies with $N = 3$ are reported, seem to indicate that indeed, even for $N = 3$ such number is unbounded. Figure 3 shows a choreography with $N = 3$ which belongs to a family which seems to contain a countable set of non-equivalent elements. Work to obtain a theoretical proof is in progress. The key idea is that this family is associated to a transversal heteroclinic connection between two invariant objects at infinity, like in the Sitnikov problem. But now we are dealing with the general 3-body problem and all the dimensions and technicalities are more involved.

(C) From (10) it is clear that the equations are not defined beyond a time $t = t^*$ when two, at least, of the bodies tend to the same position at that time. Assume that this occurs for a solution φ as t increases towards t^*. Then we say that a collision occurs for $t = t^*$ along φ. However one can ask if there is some way to "continue" the solution φ across the collision. That is, whether or not there exists another solution, ψ, ending to the same collision when t decreases to t^* and such that if we extend the solution φ by ψ one recovers continuity with respect to initial conditions. See [18] for a survey on this problem.

It has been proved that, in general, collisions involving three or more bodies cannot be regularised, while all collisions which involve only binary collisions (perhaps some of them simultaneously) can be regularised. Then the problem is to characterise how regular is the extension of φ by ψ.

[1] Preliminary numerical explorations for equal or near equal masses, suggest that for N=6 there are 3624 solutions, for N=7 there are 53640 and for N=8, 696240 RES are found.

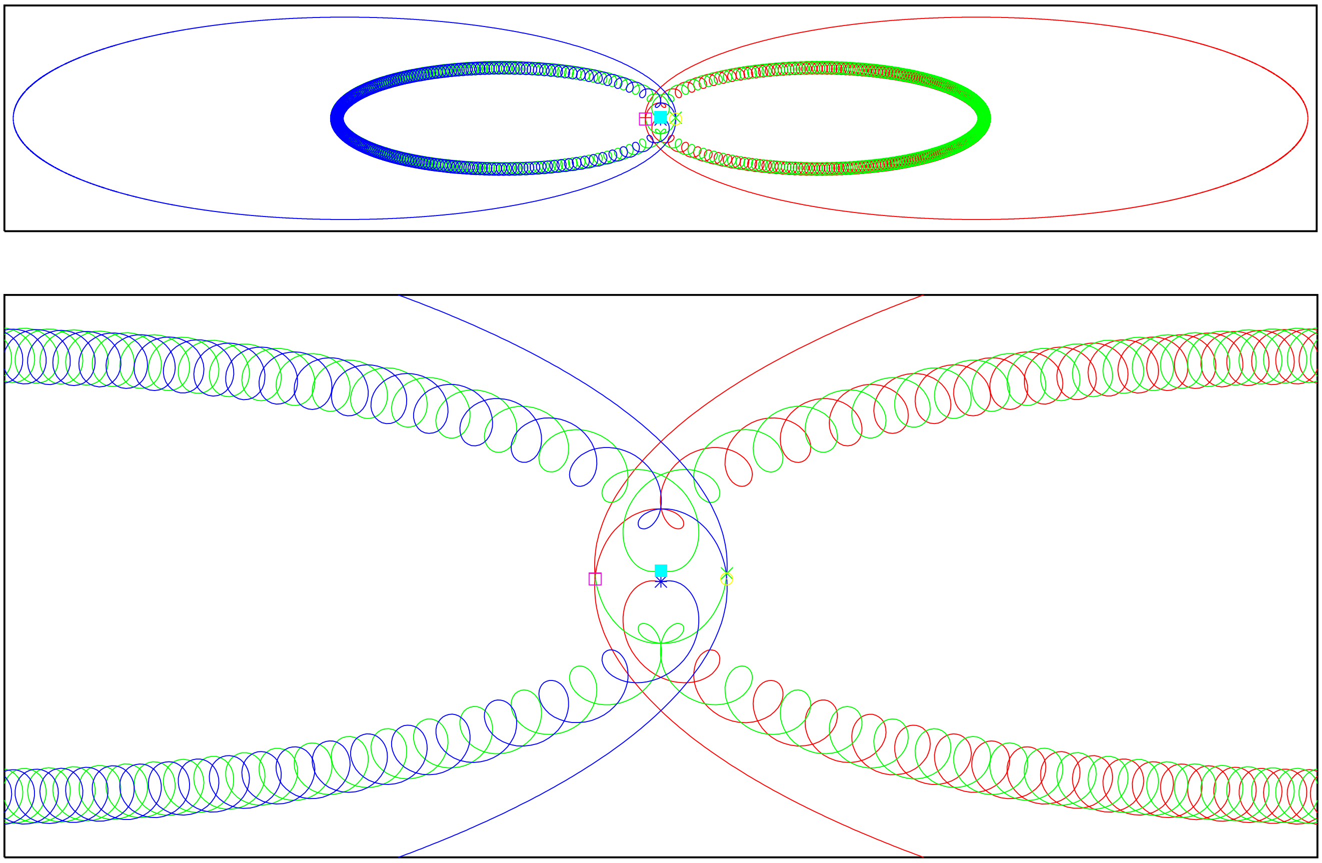

Figure 3: Top: A choreography of the 2-body problem. Three equal masses move in a periodic orbit along the same path. Bottom: A magnification of the central part. In each one of the binary portions, the bodies in the binary make 200 revolutions around their centre of masses.

That is, assume one takes an analytic section, Σ_{in}, transversal to the solution $\varphi(t)$ at some t_{in}, with $t^* - t_{\text{in}}$ small and $t_{\text{in}} < t^*$. In a similar way one takes a section, Σ_{out}, transversal to ψ at some t_{out}, with $t^* - t_{\text{out}}$ small and $t_{\text{out}} > t^*$. We ask for the differentiability of the map T passing from Σ_{in} to Σ_{out} along the flow.

This involves several unstable and stable manifolds along the so-called "collision manifold". Several numerical studies, reported in [16] suggested that the map is exactly $\mathcal{C}^{8/3}$ unless the involved masses take some special values. This was proved later in [17].

From the numerical point of view to recognise the regularity of a function, that is, how differentiable it is, is always a delicate task. But several tools allow to obtain quite coherent results (see e.g. [3] and [16]).

(D) Applications of invariant objects play also a key role in the design of orbits for space missions. The references [12, 11] contain the reproduction of technical reports written for the European Space Agency in the period 1983–1993. The methodology to obtain invariant objects and their associated invariant manifolds was applied, in these projects, to space science. See also [23, 26] for further information and other applications.

With these tools the design of missions involving successive passages of a spacecraft near a binary hierarchical system (Sun+planet or planet+satellite) becomes a routine task.

3 Exploring parameters and phase space: methodology and a first example

Usually dynamical systems depend on parameters. A key goal would be to describe the main features of the dynamics and how they evolve with parameters. This Section and next three are partly devoted to this subject.

One of the first characteristics to be studied for an orbit of a dynamical system is if it can be considered regular or chaotic. A definition in a not very restrictive sense will be given later. It is based on the Lyapunov exponents.

Typical regular orbits are, beyond fixed points, the periodic solutions and the orbits which can be seen as superposition of periodic motions with incommensurable frequencies. To look for these frequencies one uses the frequency analysis.

These two tools, Lyapunov exponents and frequency analysis, used in a complementary way, are extremely useful to determine properties of the dynamics. See [28, 30, 13] and references therein.

3.1 Frequency analysis

Assume we sample a function f, taking values in $\mathbb{C}$ at some values of time $t_0 < t_1 < \ldots < t_N$. If f is quasi-periodic with frequencies $\omega_1, \ldots, \omega_d$, incommensurable (i.e., the scalar product (k, ω) is never zero for $k \in \mathbb{Z}^d \setminus \{O\}$), it has a representation of the form

$$f(t) = \sum_{k \in \mathbb{Z}^d} a_k \exp(\mathrm{i}(k, \omega)t). \tag{11}$$

The standing question is how to recover good estimates of the frequencies and the most relevant coefficients a_k from the sample $\{f(t_0), f(t_1), \ldots, f(t_N)\}$. In many examples the epochs are equispaced: $t_{i+1} - t_i = T/N =$ constant. The most common method for this purpose is to compute the Fourier transform of the data (typically using the FFT routines) and after this the most important frequencies are detected from the peaks of the Fourier transform. Then it is possible to guess some basic frequencies $\omega_1, \ldots, \omega_d$ such that all the peaks are identified as being of the form (k, ω) for some $k \in \mathbb{Z}^d$. Note that, in general, when a time series obtained from a physical or numerical experiment is analysed, we do not know

- If it is correct to assume that the function f is quasi-periodic.
- How many rationally independent frequencies, d, has the function.
- How accurate are the frequencies and the coefficients.

The worst difficulty arises from a rough use of the Fourier transform, because then the local maxima of the FFT differ by an amount of the order of $1/N$ from the true frequencies. Other difficulties are the effect of aliasing, which can reduce the range of frequencies that one can determine. This effect can be minimised by increasing T, if possible. Harmonics having $|a_k|$ large produce a shift on the location of other nearby peaks, a difficulty which can be decreased by introducing a filter. But, in general, it is not common to produce estimates of the frequencies with small error.

In [11] a different method has been proposed and tested. It mainly consists in an iterative Newton method, to determine simultaneously the frequencies and amplitudes. See [13] for further details and references to other algorithms. If f is certainly quasi-periodic and samples of a 2^{15} or 2^{16} points are used, it is possible to recover the frequencies with error below 10^{-12}.

The constancy of the frequencies along the orbit can be used as a test to detect regular motion. Furthermore, the possible variations of the frequencies with respect to time can serve as an indication of the amount of diffusion in the system. This has been used not only to detect how far a system is from being integrable, but also to improve the design of devices like particle accelerators.

3.2 Lyapunov exponents

Lyapunov exponents measure the mean value of the exponential rate of increase of the distance between nearby orbits. For concreteness assume T is a diffeomorphism in $\mathbb{R}^m$ with bounded orbits like (3). Similar formulations work in the case of ODE like (1). Let x_0 be an initial point and $x_n = T^n(x_0)$, $n \in \mathbb{Z}$ its orbit. Given a vector $\xi \in \mathbb{R}^m$, $\|\xi\| = 1$ consider

$$\lim_{k\to\infty} \log(\|DT^n(x_0)\xi\|)/n. \tag{12}$$

The limit exists for almost all x_0 and ξ and, with probability 1, gives the maximal Lyapunov exponent.

The geometrical meaning is easy to understand: regular orbits have a mild local instability. Nearby orbits can diverge but only at a rate which is linear (or, at most, polynomial) with respect to the number of iterates (or with respect to time for ODE). Hence the limit in (12) is zero. On the other hand chaotic or irregular orbits are characterised by a local exponential divergence and then the limit is positive. It is quite often taken the positiveness of the Lyapunov exponent as synonymous of chaos (despite this is not completely correct).

In fact, the first k Lyapunov exponents can be computed with the algorithm that we describe now.

Let $\xi_0^j, 1 \le j \le k$ be random initial vectors. From them one can obtain orthonormal vectors, again denoted as ξ_0^j. Initialise $y_0^j = 0$ for $1 \le j \le k$. After m steps of the algorithm we proceed to the next one. The images

$$\eta_{m+1}^j = DT(x_0)\xi_m^j, \quad 1 \le j \le k$$

are computed and then orthogonalised (not yet normalised) to obtain vectors ζ_{m+1}^j. The values of the y^j are updated by

$$y_{m+1}^j = y_m^j + \log(\|\zeta_{m+1}^j\|)$$

and finally we compute the next values of the ξ^j vectors by

$$\xi_{m+1}^j = \zeta_{m+1}^j/\|\zeta_{m+1}^j\|, 1 \le j \le k.$$

Then the estimates of the first k Lyapunov exponents after n iterates are obtained from

$$\ell_n^j = y_n^j/n, \quad 1 \le j \le k.$$

The values of ℓ_n^j converge to limits ℓ^j when $n \to \infty$ with probability 1. In particular ℓ^1 coincides with the result of (12).

This standard procedure has the problem of a slow convergence to zero in case of a regular motion. This can be overcome by different procedures, see [9, 8]. These methods are used in the example which follows and also in next Sections.

3.3 An standard–like map

This is an introductory example. A simplified version of this map (the so-called standard or Chirikov map) is often used as an illustration of the behaviour of different dynamical indicators.

Let us define, in the two-dimensional torus $\mathbb{T}^2$, the map

$$T_{\varepsilon,\mu,\varphi}\begin{pmatrix} x \\ y \end{pmatrix} = \begin{pmatrix} \bar{x} \\ \bar{y} \end{pmatrix} = \begin{pmatrix} x+\varepsilon\bar{y} \pmod{2\pi} \\ y+\varepsilon f_{\mu,\varphi}(x) \end{pmatrix}, \tag{13}$$

where $f_{\mu,\varphi}(x) = g_{\mu,\varphi}(x) - \bar{g}$, $g_{\mu,\varphi}(x) = \frac{\sin(x+\varphi)}{1-\mu\cos(x)}$ and $\bar{g}$ denotes the average of g. It is not entire (in contrast with the Chirikov map) and contains all the harmonics at once. The role of φ is to break the symmetry.

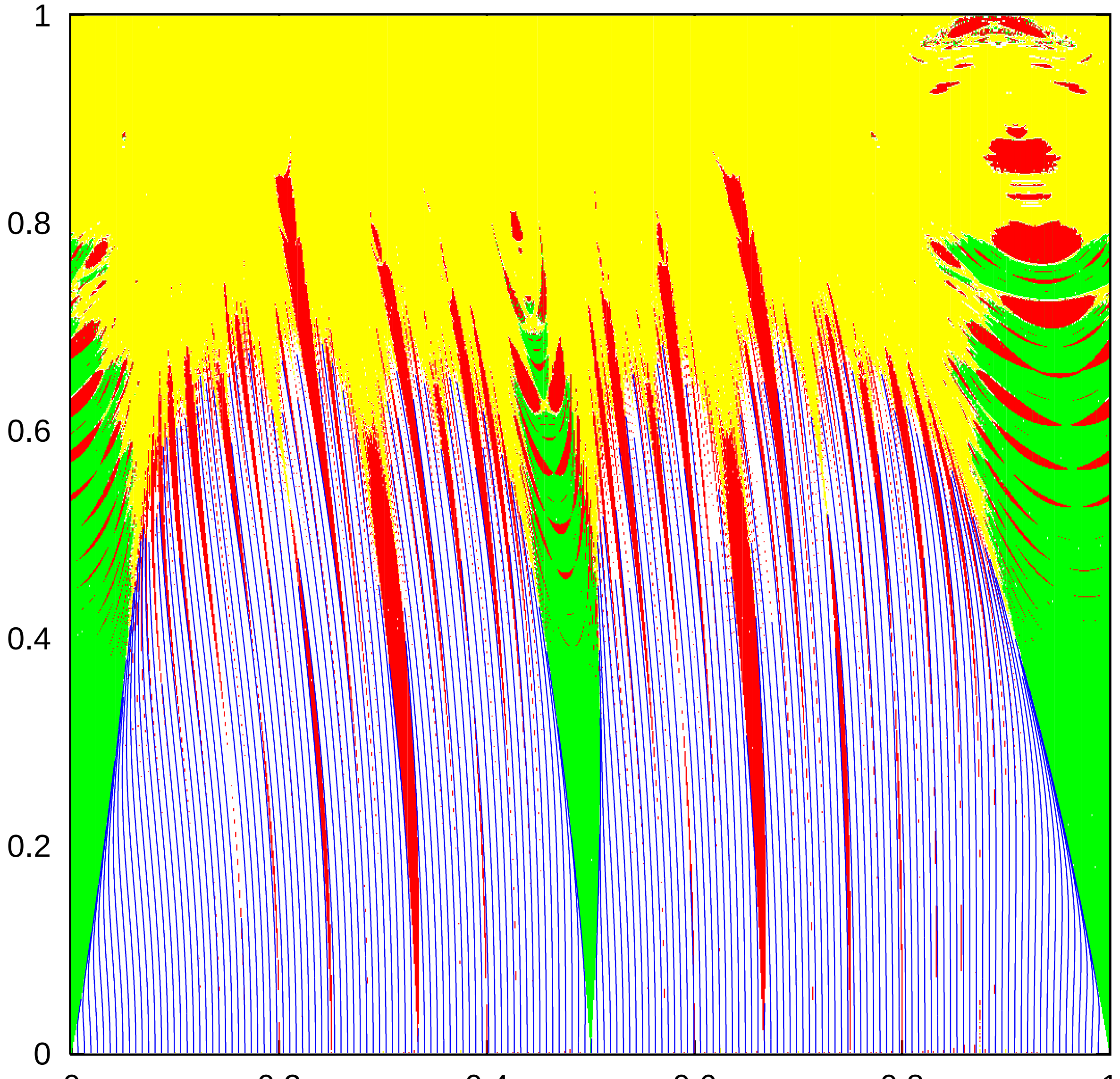

Figure 4: Diagram action–perturbation parameter for an standard-like map. Colour code: green: the 1-to-1 and 2-to-1 resonances; red: higher order resonances and zones of islands inside the 1-to-1 and 2-to-1 resonances; yellow: chaotic zone; blue lines: they correspond to invariant curves. See the text for details.

For $x_0 = 0$ and the initial action variable $y_0 \in [0, 2\pi]$, different values of the perturbation parameter $\varepsilon \in [0, 1]$ have been scanned, looking for regular ($\ell^1 = 0$) or chaotic ($\ell^1 > 0$) motion. Furthermore frequency analysis has been used to check also regularity and to detect the different resonances. Resonances of the form p/q with $q = 3, 4, 5, 6, 7$ and higher are clearly seen. The resonances whose associated areas go to larger values of ε (beyond $\varepsilon = 0.8$) correspond to $2/7$ and $5/7$.

Figure 4 shows some results for $\mu = 0.5$, $\varphi = 1$. In the horizontal (resp. vertical) axis the variable $y/(2\pi)$ (resp. ε) is shown. The yellow parts on the top correspond to $\ell^1 > 0$, all other values having $\ell^1 = 0$.

Furthermore, using the methods to obtain invariant curves explained in Section 2, we have computed the location of the y variable of different invariant curves, when they intersect $x = 0$, as a function of ε. All points in one of the lines in blue in the figure have the same rotation number. This would be the value of ω in (5). The values used are of the form

$$m\gamma/100, \qquad 1 \le m \le 161, \qquad \gamma = \frac{\sqrt{5}-1}{2},$$

that is, rational multiples of the golden mean. The blue curves begin at $\varepsilon = 0$ and stop at different values of ε, when the invariant curves become destroyed.

The diagram shown in Figure 4 is an easy way to describe most of the dynamics of the map and the dependence with respect to ε. Unfortunately in more interesting cases, when the number of relevant variables and parameters is higher, the representations have to be presented in a different way, by means of sections or slices.

4 Unfolding degenerate cases

Invariant objects with some degeneracy play an important role as organising centres when we change parameters. We shall consider the case of fixed points x^*. For autonomous ODE this occurs when some eigenvalue of the differential of the vector field, $Df(x^*)$, has eigenvalues with zero real part. For maps when $DT(x^*)$ has eigenvalues with modulus 1. Given a condition of degeneracy for an ODE, in terms of values of some eigenvalue of $Df(x^*)$, the corresponding condition for maps is the exponential of the condition for ODE. It is not restrictive to suppose $x^* = 0$. Assume a system with a degenerate fixed point belongs to a family of systems with parameter $\mu \in \mathbb{R}^d$. It is again not restrictive to suppose that the degeneracy occurs when $\mu = 0$. The standing question is: Which kind of things can occur in a neighbourhood of $x = 0$ when small changes of μ are done?

This can be studied for concrete families, but a more ambitious goal can be to try to describe all possible patterns of the dynamical system near that fixed point for arbitrary families of perturbations. The study depends on how degenerate the fixed point is, that is, how many eigenvalues have real zero part (resp., have modulus 1) for vector fields (resp. for maps) and on some of the nonlinear terms of the system. Assume that a given family f_α or T_α with $\alpha \in \mathbb{R}^p$ is able to display all possible dynamics of a general family f_μ or T_μ. Then we say that f_α or T_α "unfold" the degeneracy: It is enough to study this family to see all the possible things which can occur.

Only very simple degeneracies can be unfolded in this way. For higher order degeneracies, and when the dimension of the space (in the case of ODE) exceeds 2, it can happen that the richness of the system is such that the unfolding parameter α must have infinitely many components. But we can restrict our ambition to describe the most relevant facts which can occur, without entering into too subtle details. Then it can be possible to produce finite dimensional unfoldings which account for the description of the most important patterns of the dynamics of any perturbation.

To be concrete we shall confine to a double degeneracy of the so-called Hopf-saddle-node type (HSN for short). For vector fields this means that one eigenvalue is zero (saddle-node) and that, simultaneously, a couple of complex eigenvalues have zero real part (Hopf). Moving parameters in a suitable way the fixed point can disappear or it can split in two different fixed points. Moving in another way a family of periodic solutions can emanate from the fixed point. This will be a family of invariant curves in the case of maps. This is what can occur if no higher order degeneracies are present. The complications of the dynamics arise from the coupling of these two bifurcations.

To study this kind of problems one has to begin by introducing suitable normal forms. That is, we do changes of variables to try to simplify, as much as possible, the equations at hand without changing the dynamics. Which one is the normal form for a given system depends of the objects in which we are interested. Then the general methodology is

- Compute the normal form, depending on all variables (i.e., state space variables and parameters) up to a suitable order, say r.
- Truncate the normal form to order r and study the resulting system. Prove the existence of the objects in which we are interested.
- Show that these objects subsist when the remainder of the normal form (i.e., the terms of order greater than r, neglected in the previous step) are taken into account.

An important thing to remark is that in the passage from the second to the third item some differences can occur. There are phenomena which can occur for the system and which are not seen in the normal form for any value of r. They are called phenomena beyond all orders (of normalisation). Other techniques have to be used to detect them.

4.1 The Hopf-saddle-node bifurcation

We consider first the case of vector fields and then we pass to diffeomorphisms. Start with a vector field like

$$X(\alpha) = \begin{pmatrix} f_{000}(\alpha) + (\mu(\alpha) + \mathrm{i}\omega(\alpha))w + \Sigma f_{jkl}(\alpha) w^j \bar{w}^k z^l \\ g_{000}(\alpha) + \nu(\alpha) z + \Sigma g_{jkl}(\alpha) w^j \bar{w}^k z^l \end{pmatrix} \tag{14}$$

where $j, k, l \geq 0$, $j + k + l \geq 2$, $f_{jkl}(\alpha) \in \mathbb{C}$, $g_{jkl}(\alpha) \in \mathbb{R}$. The complex variable w denotes $x + \mathrm{i}y$ and we consider (x, y, z) as coordinates in $\mathbb{R}^3$. The parameter α belongs to $\mathbb{R}^k$, $k \geq 2$. A preliminary step has been to put the linear terms in a simple form. We assume that for $\alpha = 0$ we are exactly at the HSN, that is:

$$f_{000}(\alpha) = 0, \quad \mu(\alpha) = 0, \quad g_{000}(\alpha) = 0, \quad \nu(\alpha) = 0.$$

Furthermore we assume that some generic conditions hold, that is, some higher order terms are different from zero. Otherwise we have a stronger degeneracy.

Then the vector field in (14) can be put, by changes of variables and eventual time reversing, in the form

$$\frac{\mathrm{d}}{\mathrm{d}t}\begin{pmatrix} w \\ z \end{pmatrix} = Y + O(||w, z||^4), \qquad Y = \begin{pmatrix} (-\beta_2 + \mathrm{i}\omega)w + awz - wz^2 \\ -\beta_1 - sw\bar{w} - z^2 \end{pmatrix}, \tag{15}$$

where $\beta = (\beta_1, \beta_2) = \beta(\alpha)$ are two new parameters which are the only ones which play a role up to this order, $a = a_1 + \mathrm{i}a_2 \in \mathbb{C}$ and $s = \pm 1$. We remark that the normal form up to order 3 given by the vector field Y in (15) has rotational symmetry. It is invariant by rotations in the w (or (x, y)) plane. In particular, if $\beta_1 < 0$, $s = 1$ it has two fixed points, located at $w = 0$, $z = \pm\sqrt{-\beta_1}$, and there is an orbit, on $w = 0$, connecting them, that is, an heteroclinic connection. This property is preserved to any order of normalisation. This makes the discussion of the behaviour of Y quite simple, but we should be aware that a vector field as in (14) can have some types of phenomena that are not seen in Y. They depend on the exact form of X and not in any of their approximations. Usually they are called "algebraically undetectable" because they cannot be read from any finite part of the power series expansion of X in the case of analytic vector fields.

To illustrate this we shall consider a quite simple example. This is the classical Kuramoto-Sivashinsky equation in the conservative case,

$$\begin{array}{l} p' = q \\ q' = r \\ r' = f \end{array}, \qquad \text{or simply} \qquad p''' = f, \qquad \text{where} \qquad f = -1 + ap + q^2 = -1 + ap + (p')^2. \tag{16}$$

After scaling variables and parameter, and some nonlinear transformations, (16) can be put in the setting of (14). The HSN occurs (in the present parameter a) when $a \to -\infty$. In the variables of (15), and any order of normalisation, there is an heteroclinic connection between two fixed points: One of the branches of the unstable manifold of one of the fixed points coincides with one of the branches of the stable manifold of the other fixed point. However it can be proved that this connection does not occur for any $a < a_0$ if $a_0 < 0$ and $|a_0|$ is sufficiently large. In fact, the distance between the invariant manifolds above mentioned, measured on the plane orthogonal to the segment joining the fixed points and passing through the middle point, is of the form $2d(a)$ where

$$d(a) = K(a)|a|^4 \exp(-\frac{\pi}{2}|a|^{3/2}), \qquad \text{where} \qquad K(a) = K(0) + O(|a|^{-3/2}).$$

When $a < 0$ and $|a|$ is large, this is really a very small distance. For instance, for $a = -10^{8/3}$ the estimated value of $d(a)$, computed using the methods of Section 2, working with 7900 decimal digits is

$$10^{-6816} \times 0.478612665881755572964626887390674523...$$

which has been computed with (at least) 1000 correct significant digits. See [10] for theoretical results and the dynamical consequences.

We turn now to the case of HSN diffeomorphisms. The situation is much more involved. Beyond their theoretical interest this bifurcation is one of the organising centres to understand the so called Lorenz-84 climate model with seasonal forcing, see [4]. By changing parameters in this simplified global climatological model (a system in $\mathbb{R}^3$ with time periodic coefficients), which takes into account the seasonal effect of the Sun, all the richness of the HSN for 3D diffeomorphisms shows up.

In a similar way to what is done for the vector field, one can obtain the normal form. But now changes of time are not admissible. Hence we obtain

$$\begin{pmatrix} w \\ \bar{w} \\ z \end{pmatrix} \mapsto \begin{pmatrix} f_{100}w + f_{101}wz + f_{102}wz^2 \\ \bar{f}_{100}\bar{w} + \bar{f}_{101}\bar{w}z + \bar{f}_{102}\bar{w}z^2 \\ g_{000} + z + w\bar{w} + z^2 + g_{003}z^3 \end{pmatrix} + O_4, \tag{17}$$

where $f_{100}, f_{101}, f_{102} \in \mathbb{C}$, $g_{000}, g_{003} \in \mathbb{R}$, being $|f_{100} - \lambda|$ and $|g_{000}|$ small. As the normal form has too many parameters, even truncated skipping the fourth order terms, one can use a different approach:

- To introduce suitable scalings in the region of interest. The most interesting situation occurs when $\beta_1 < 0$ and $s = 1$. Hence we define γ and δ_2 by $\beta_1 = -\gamma^2, \quad \beta_2 = \gamma^2\delta_2$. Then the variables w, z are scaled by γ (but we keep the same name after scaling),

- To construct model diffeomorphisms by taking the time γ flow of (15), looking at the vicinity of a resonance with detuning term $\gamma\delta_1$, that is, taking $\omega = 2\pi(p/q + \gamma\delta_1)$,

- To keep resonant terms in the normal form (in contrast with the vector field case these terms cannot be skipped now) and add some term to destroy the rotational symmetry, which still subsists for the normal form of the diffeomorphisms.

The result are models of the form

$$R : \begin{pmatrix} w \\ z \end{pmatrix} \mapsto \begin{pmatrix} e^{2\pi \mathrm{i}(p/q+\gamma\delta_1)} w[1-\gamma(\gamma\delta_2 + az + \gamma z^2)] \\ z + \gamma(1-|w|^2 - z^2) \end{pmatrix} + \begin{pmatrix} \gamma^3(\varepsilon_1 \bar{w}^4 + \varepsilon_2 z^4) \\ \gamma^4 \varepsilon_3 \operatorname{Re}(w^5) \end{pmatrix}, \tag{18}$$

where now $a = a_1 + \mathrm{i}a_2, \varepsilon_2 \in \mathbb{C}$ and $\varepsilon_1, \varepsilon_3 \in \mathbb{R}$ are finite coefficients and $\gamma, \delta_1, \delta_2 \in \mathbb{R}$ are small parameters. The models (18) are compared to (17). Most of the parameters appearing in 17) are found in (18), either directly or in an equivalent form, and it has been checked that the ones which do not appear have a small influence. The finite coefficients in (18) have been fixed to suitable values. The choices made are $a = -1 + \frac{\mathrm{i}}{\sqrt{2}}$, $\varepsilon_1 = \varepsilon_2 = 1$, $\varepsilon_3 = 0$, $p/q = 1/5$. See [5] for a discussion.

Finally, only the parameters $\gamma, \delta_1, \delta_2$ are left as free parameters to explore the maps numerically. For theoretical analysis all the parameters are left in literal form. Furthermore different tests have been done with γ. Typical explorations have used $\gamma = 0.1$, 0.05, 0.02, 0.01. Changing γ essentially amounts to rescale the bifurcation diagram. Of course, different phenomena scale in different ways. Results are presented for $\gamma = 0.1$ for better visibility.

Figures 5 and 6 show the output of computations of the Lyapunov exponents, denoted here $\lambda_1 \geq \lambda_2 \geq \lambda_3$, for model (18) as a function of δ_2 and δ_1. Different colours correspond to different ranges of the three Lyapunov exponents, as explained in the caption. The dynamical meaning is:

- Some positive Lyapunov exponent denotes existence of a strange attractor.

- Two exponents equal to zero and a negative exponent corresponds to an attracting $\mathbb{T}^2$.

- One exponent equal to zero and two negative corresponds to an attracting curve. It is transversally of focus type if $\lambda_2 = \lambda_3$. Otherwise it is of node type.

- All negative exponents corresponds to attracting periodic points. Different types of exponents tell us, then, the local behaviour near these points.

It has to be remarked that several attractors can (and do) exist for the same δ_1, δ_2. The plot corresponds to a particular one. It depends on the initial condition used to start the iterations. Proofs of this fact and existence proofs of curves, tori and bifurcations in some domains can be found in [5].

The interaction of the dynamics due to the rotational part (the term in $\exp(2\pi\mathrm{i}(p/q+\gamma\delta_1))$ in (18)) with the rotation which appears in cylindrical coordinates in (15), that is: $r' = w(\gamma\delta_2 + a_1 z + \gamma z^2)$, $z' = -1 + z^2 + r^2$, produces a dense set of resonances. When they occur the motion in a $\mathbb{T}^2$ becomes phase-locked. The torus still exists but has only finite differentiability (see [3]) despite the map is analytic. Inside the torus there are attracting and repelling analytic invariant curves. In the lower part of Figure 6 we display the computed part of such a network. Only resonances with a width of the order of one pixel are seen.

In the complement of the resonances (a nowhere dense set) there are invariant tori with irrational dynamics. Other kinds of dynamics (e.g., with quotient of the frequencies equal to a Liouville number) appear only for sets of very small measure, both in the space of variables and in the space of parameters.

In the upper part of Figure 6 the red zone corresponds to strange attractors. The pattern in the parameter space is reminiscent of patterns which can be found for the well-known Hénon attractor.

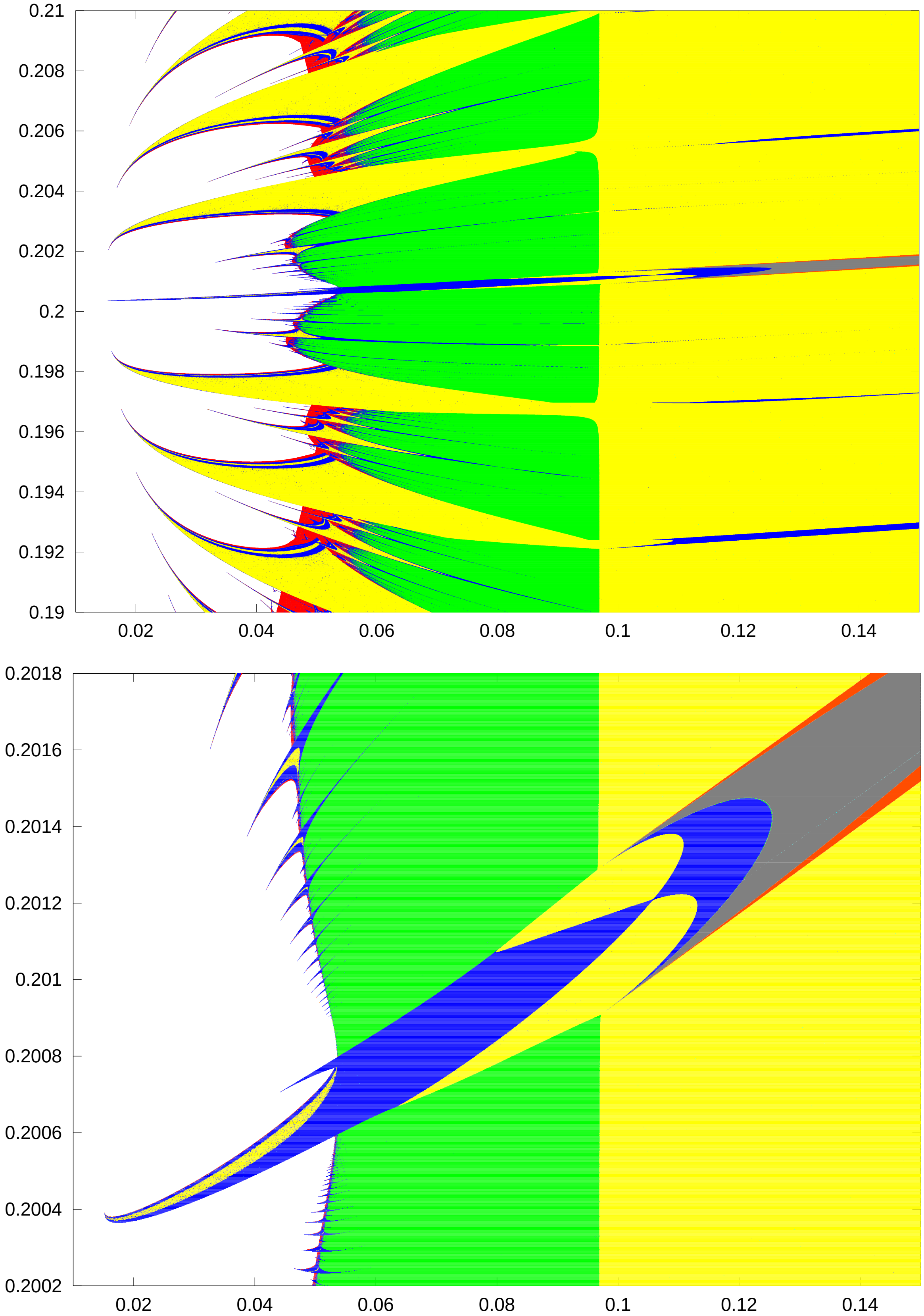

Figure 5: Exploring the behaviour of the Hopf-saddle-node bifurcation for 3D maps. The variable in the horizontal (resp. vertical) axis is δ_2 (resp. δ_1). Major colour codes: red ($\lambda_1 > 0 = \lambda_2 > \lambda_3$), green ($\lambda_1 = \lambda_2 = 0 > \lambda_3$), blue ($\lambda_1 = 0 > \lambda_2 > \lambda_3$), yellow ($\lambda_1 = 0 > \lambda_2 = \lambda_3$), grey ($0 > \lambda_1 = \lambda_2 \geq \lambda_3$), brown ($0 > \lambda_1 > \lambda_2 = \lambda_3$). See text for the dynamical meaning. Top: a general view. Bottom: a magnification near the 1-to-5 resonance.

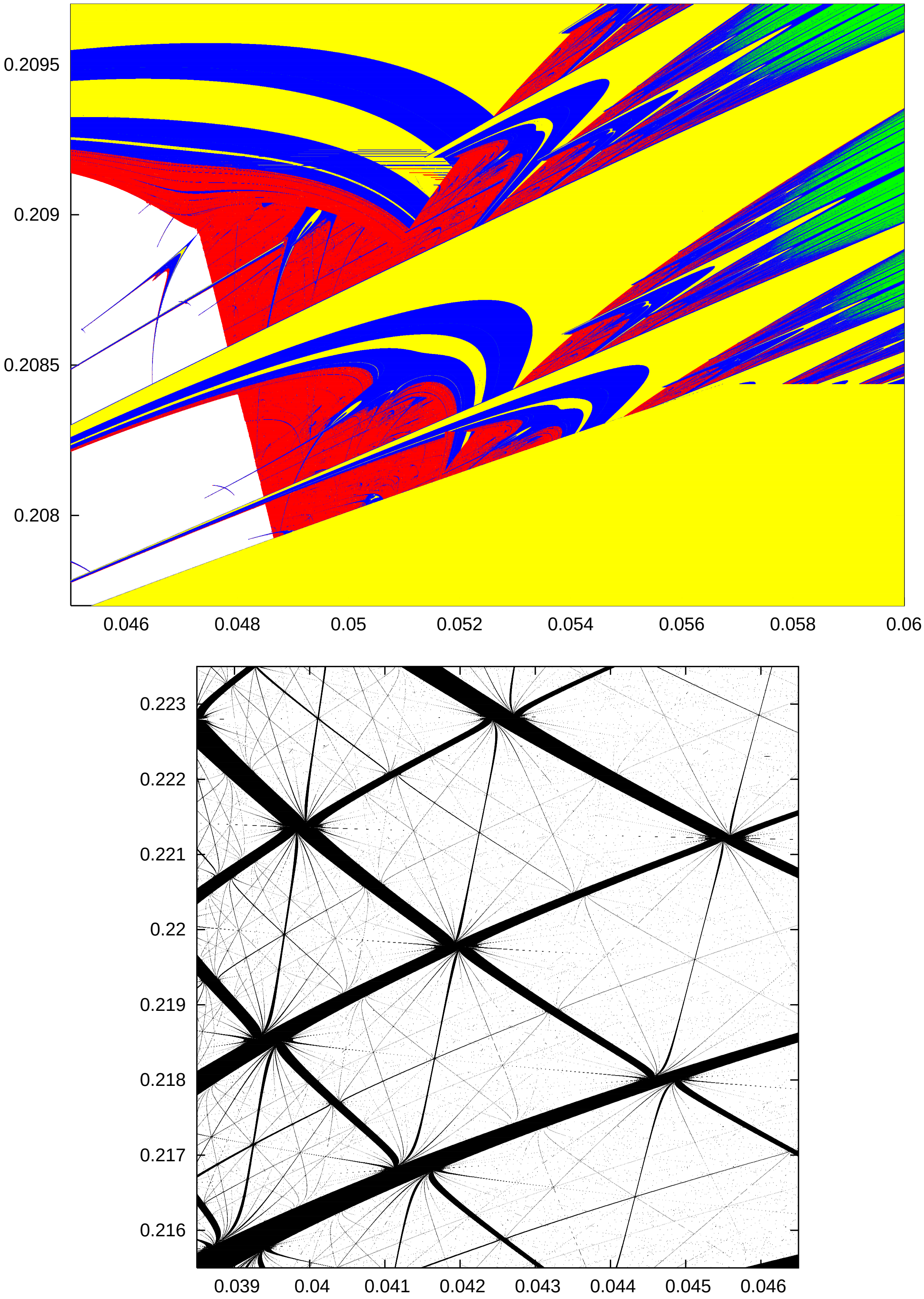

Figure 6: Top: Magnifications of Figure 5 in the zone of largest abundance of strange attractors. Bottom: Magnification of a resonant web for a slightly different map.

5 Diffusion in phase space

We shall consider now Hamiltonian systems. It is well known that (globally) integrable autonomous systems with n degrees of freedom have a very simple structure: There are n first integrals F_i, $i = 1, \ldots, n$ in involution and functionally independent except, at most, on a set of zero measure. One of the integrals can be taken to be the Hamiltonian itself. If a level set of the first integrals $F^{-1}(c)$, for some constant vector $c \in \mathbb{R}^n$, is compact and the integrals are independent on it, then $F^{-1}(c)$ is a torus $\mathbb{T}^n$. In this case it is possible to introduce, in a vicinity of this torus, action-angle coordinates and the actions are invariant under the flow. The phase space is locally foliated by invariant tori. Under generic conditions the frequencies on these tori depend on the actions.

This simple picture is destroyed when general perturbations are introduced. The actions are no longer constant, all or part of the tori are destroyed. If $n = 2$ and the perturbation is small, KAM theorem assures (under some non-degeneracy conditions) that most of the invariant tori survive. As the energy is preserved, the motion takes place in a 3-dimensional set, and the subsisting invariant tori, which are 2-dimensional, confine the motion. The variations of the actions are small.

This is no longer true if $n \geq 3$. Then the levels of energy are $2n-1$-dimensional, while the invariant tori are n-dimensional and they cannot confine. We say that the motion can diffuse in the phase space. There is a fundamental mechanism to understand how this diffusion takes place, even if the perturbation is very small (but then, certainly, the speed of variation of the actions can be extremely small). The idea is that there can be invariant tori of dimension less n or centre manifolds of these tori, which have some unstable and stable directions. We say then that there exists a normally hyperbolic invariant object. The motion in the phase space can pass near one of these invariant objects and then follow closely its unstable manifold. If this manifold intersects an stable manifold of another object then the motion comes near this new invariant object and the process is iterated. If a large chain of these connections can be found, the motion can use it to change the actions (I mean, the variables which would be the actions if the system were unperturbed) by an important amount.

Even if there are no tori, but for a nearby system (i.e., with slightly different parameters) such a chain exists, then the system "remembers" what happened for this nearby system and the chains can still subsist.

Hence, there are two ingredients to have diffusion: The first one is to have invariant tori (or other more general objects) which are normally hyperbolic. The second one is to have some connection which is transversal. Indeed, it could happen that the stable and unstable manifolds coincide and then one could not obtain a chain connecting to other distant objects. If the unperturbed system has some separatrices, they must be splitted (i.e., non-coincident) when the perturbation is introduced.

5.1 Splitting of separatrices

This is a delicate problem in many cases, because when the system is a small perturbation of an integrable one, with angles rotating at a finite (away from zero) speed and the dynamics in the hyperbolic (unstable and stable) directions is slow, the lack of coincidence of the manifold is exponentially small in the perturbation, i.e., it cannot be found by classical perturbation theory up to any order. See [24] to see the reasons for that.

One of the most studied examples is given by the Hamiltonian

$$H(y, I_2, I_3, x, \theta_2, \theta_3) = \frac{1}{2}(y^2 + I_2^2) + I_3 + \varepsilon(\cos x - 1)\left(1 + \mu(\cos\theta_2 + \cos\theta_3)\right). \tag{19}$$

It was introduce by Arnol'd in 1964, with two parameters, ε and μ, but μ assumed to be extremely small with respect to ε. Now consider both of them equal. One can see [31] for motivation, additional references and technical details.

Here the unperturbed Hamiltonian contains the terms of degrees 0 and 1 in ε, while the terms in ε^2 are the perturbation. Furthermore, the entire character of the perturbation $(\cos x - 1)(\cos\theta_2 + \cos\theta_3)$ adds more difficulties, because the splitting of the separatrices of the hyperbolic tori ($x = y = 0$, I_2 fixed and $(\theta_2, \theta_3) \in \mathbb{T}^2$), becomes much smaller than in a general analytic case.

Assume we are interested in the vicinity of $I_2 = \omega$. Scaling and shifting variables and time and introducing $\eta = \sqrt{\varepsilon}$ we obtain the system

$$\begin{aligned} x' &= (\eta + \eta^3(\cos\theta_2 + \cos\theta_3))\sin x\,, & y' &= \eta x\,, \\ \theta_2' &= \omega + \eta J_2\,, & J_2' &= \eta^3(\cos x - 1)\sin\theta_2\,, \\ & & \theta_3' &= 1. \end{aligned} \tag{20}$$

We want to have an idea of the global properties of (19) and how the effect of the splitting of separatrices is seen in some representation. We can start at the Poincaré section $x = \pi$, select $J_2 = 0$ (this is irrelevant because we can change ω) and take as parameters the initial value of y and ω. The only restriction we impose is that we take the initial value of $\theta_3 (= t)$ as zero. The splitting depends strongly on the arithmetic properties of ω. In particular, if we select ω to be the golden mean, the maximal distance (on the Poincaré section and looking at the first intersection of the manifolds with this section) is of the form

$$d(\eta) = \exp\left(-g(\eta)\frac{|\log\eta|^{1/2}}{\eta^{1/2}}\right) \tag{21}$$

if η is small enough. The function g has positive upper and lower bounds (see [31]).

To decide about the domain of regular and chaotic dynamics for system (20) we shall use the maximal Lyapunov exponent. As we are dealing with a vector field, instead of a map, the method proposed in Section 3.2 has to be slightly modified. Instead of using the differential of the map, we transport an initial vector ξ by the variational flow along an orbit of (20). We replace also the number of iterates n by a final time T. See [9, 8] for a description of the method used.

The orbit used to transport ξ enters different regions where the local rate of divergence of nearby orbits is very different. This would suggest not to take values of T too large. One of the typical unpleasant problems, in this context, is that the orbit can spend long periods of time, in a quasi-random way, close to invariant objects (invariant curves or tori, known to be sticky). Then the estimates of ℓ^1 can seem to converge to zero for a while.

The computation of the maximal Lyapunov exponent has been done for system (20) for a sample of $\eta \in [0.1, 0.3]$. In Figure 7 top, a result is presented. It corresponds to $\varepsilon = 0.0625$ ($\eta = 0.25$). The algorithm has been applied to an equispaced grid of 2000×2000 pixels in the domain $(y, \omega) \in [0, 5] \times [0, 2]$. The initial values of the remaining variables have been given above. The value $T = 10^4$ has been used. The value of η is large. This has been done on purpose, to have a very rich resonant structure.

Points in green correspond to regular behaviour (ℓ^1 essentially equal to zero), while points in red correspond to chaotic behaviour (ℓ^1 definitely positive). The intermediate range is considered as, possibly, mildly chaotic. The values of the thresholds have been selected to have a good contrast between both kinds of orbits.

There is a large chaotic zone close to $y = 2$. This is the right boundary of the main resonance. Between $y = 0$ and $y = 2$ there is large set of points in green, corresponding to regular motion inside the resonance, but secondary resonances cross this regular domain. The same pattern can be seen to the right of $y = 2$. A complicated pattern of resonances appears. In particular a large resonant zone shows up, in a vertical direction, to the right of $y = 4$. It corresponds to a 1-to-1 resonance between the mean motion of the x and θ_3 variables.

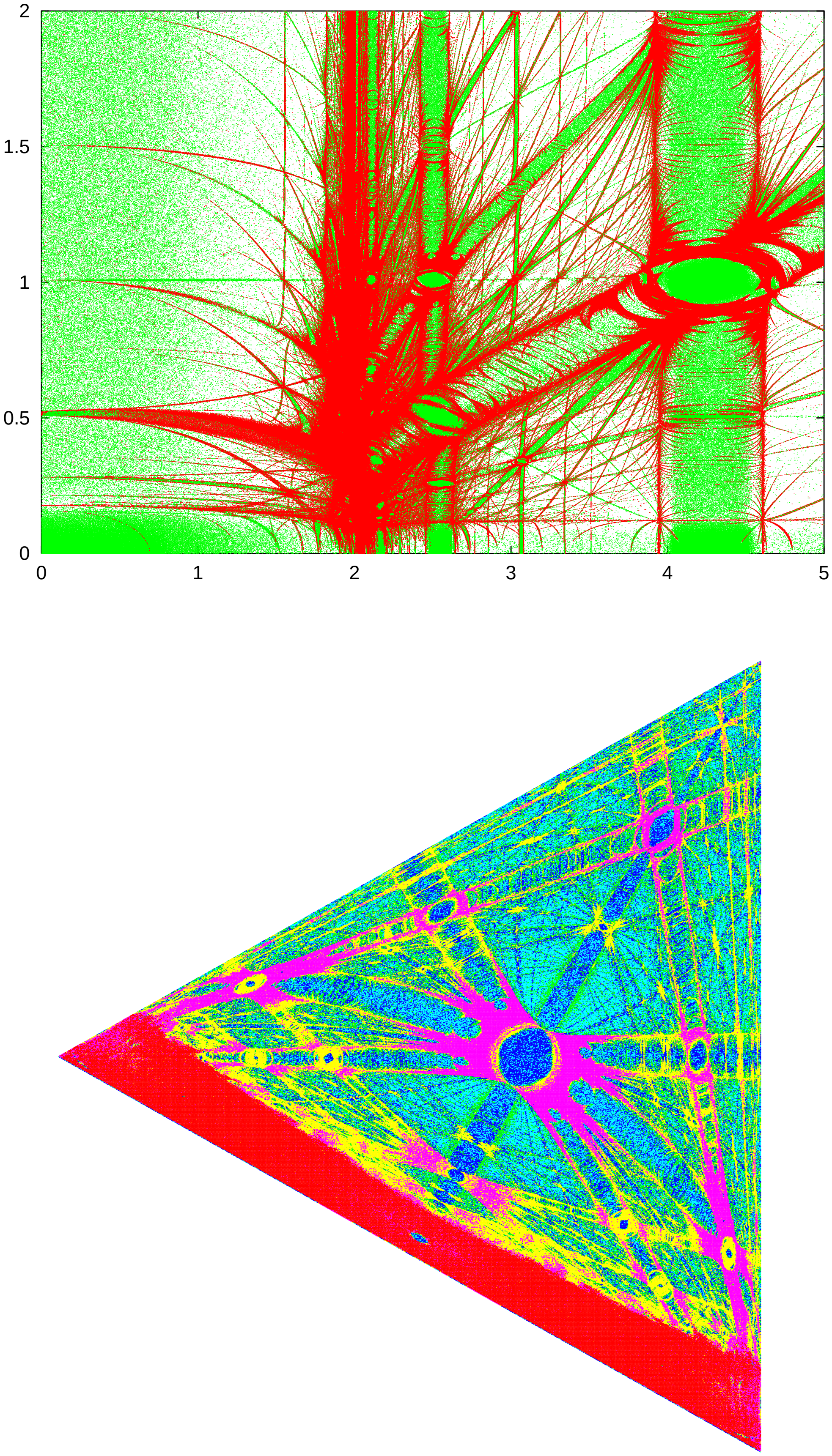

Figure 7: Resonance channels playing the most relevant role in diffusion. Top: the classical Arnold example of diffusion with $\varepsilon = \mu = 0.0625$. Bottom: A system of three coupled quartic oscillators. See the text for details.

5.2 Resonance channels

In the previous Figure one can see many resonant channels. The explanation for this system is easy and appears as a paradigm for a general case.

In the unperturbed case (i.e., if be delete only the terms in η^3 in (20)) $y = 0$ (resp. $0 < y < 2$, $y = 2$, $y > 2$) corresponds to the elliptic fixed point (resp. the libration orbits, the separatrix, the circulation orbits) of the pendulum part. We recall that the section has been taken on $x = \pi$. The "external" frequencies are now ω and 1. The resonances occur for the pendulum periodic orbits (either of libration or circulation type) whose frequency $\nu(y, \eta)$ satisfies $k_1\nu + k_2\omega + k_3 = 0$, $k_1, k_2, k_3 \in \mathbb{Z}$. All of them have zero width and are located on horizontal lines (if $k_1 = 0$), on vertical lines (if $k_2 = 0$) and on a countable set of curves $\omega = (-1/k_2)(k_1\nu + k_3)$, otherwise. We recall that $\nu(y, \eta) \to 0$ as $y \to 2$. This explains the general pattern of the resonances.

The "centre line" of each resonance channel corresponds to 2D (normally) elliptic tori, while the "boundary lines" corresponds to 2D hyperbolic tori. When two resonances cross there is a periodic orbit at the "centre" of the crossing. If the centre of the crossing is seen as a zone of regular motion the periodic orbit is of totally elliptic type.

The bottom part in Figure 7 describes the behaviour of another model. This is a set of three coupled quartic oscillators, but qualitatively is very similar to galactic models (see [8] for motivation and details). The coupling becomes zero on some surface of the configuration space. On this surface the total energy is the sum of the energies of the three oscillators. Hence, one can represent these energies as the barycentric coordinates of the points in a triangle. More concretely, the system has a Hamiltonian

$$H(\mathbf{p}, \mathbf{q}) = \frac{\mathbf{p}^2}{2} + \frac{1}{4}(x^4 + y^4 + z^4) + \varepsilon x^2(y + z), \qquad \mathbf{q} = (x, y, z). \tag{22}$$

Using this model and representation, the maximal Lyapunov exponent has been computed on a grid of values of the individual energies on the plane $x = 0$. The initial values of y, z are also taken equal to 0. Figure 7 bottom displays the results for $\varepsilon = 0.02$. Different levels of the Lyapunov exponent in the pixels of the plot correspond to the transition from regular to chaotic behaviour, with the colour coding: dark blue, light blue, green, yellow, violet, red, by increasing order of the exponent. The blue and green zones correspond to essentially regular motions.

Diffusion, if it occurs, has to take place along the channels seen in the Figure. When two channels cross it is possible that the orbit moves from one channel to a different one. However not all the transitions occur with a similar probability. Starting near a chaotic zone close to a given resonance it can take a very long time to visit most of the chaotic zones. This is the subject of active current research.

A similar analysis can be done for other problems which can be well approximated by Hamiltonian systems with 3 degrees of freedom. Particle accelerator designers and many other scientist start to benefit from these tools from dynamical system theory.

5.3 Small divisors

As mentioned in Section 5.1, the splitting, which is essential for diffusion, depends strongly on arithmetic properties of the frequencies. See [24] for the relation with averaging theory and [31] for a conjecture on the splitting like in equation (21) for different frequencies.

The relevant property is how close is a set of frequencies to be resonant. Assume, for concreteness, that we deal with three frequencies, ω_1, ω_2 and ω_3, and that they are non-resonant, that is, if a linear combination $(k,\omega)=k_1\omega_1+k_2\omega_2+k_3\omega_3=0$ with $k_1,k_2,k_3\in\mathbb{Z}$ then one should have $k_1=k_2=k_3=0$. But the set of all $(k,\omega), k\in\mathbb{Z}^3$ is dense in $\mathbb{R}$.

The "good" frequencies are the ones satisfying a Diophantine condition. That is, there exist positive values c,τ such that

$$|(k,\omega)|\geq\frac{c}{|k|^{\tau}},\qquad \text{for all}\qquad k\in\mathbb{Z}^3\setminus\{0\},\qquad |k|=|k_1|+|k_1|+|k_1|. \tag{23}$$

Given a fixed $\tau>2$ all values of ω, except a set of zero measure, satisfy condition (23) for some positive c.

If we look for an invariant object, like a torus, solving for equation (5) in Section 2, there appear some linear combinations of frequencies as denominators in different expressions. Even if ω satisfies a Diophantine condition, these denominators can be as small as we want (taking $|k|$ large enough). They are known as "small divisors" and are a source of problems. To detect the worst of them (which are also associated to the closest resonances) one has to look for $k\in\mathbb{Z}^3$ such that, despite $|(k,\omega)|\times|k|^{\tau}\geq c$, the product is not too far from c.

However, in contrast with the case of two frequencies, ω_1 and ω_2, there is no algorithm comparable to the continued fraction expansion of ω_1/ω_2 when three or more frequencies appear. An efficient method was presented in [25]. Assume we want to keep all k with $|k|\leq N$ such that $|(k,\omega)|\times|k|^2$ is greater than some number α. If N is small, any rough algorithm can do this in short time. However, if $N=10^8$, for instance, the computing time can be too large. An obvious reduction is to consider (5) divided by ω_3, for instance. Let $\nu_i=\omega_i/\omega_3,\ i=1,2$. It is enough to compute $\beta=k_1\nu_1+k_2\nu_2$ and then k_3 should be taken as the closest integer to $-\beta$. But the effort is still proportional to N^2.

A better algorithm proceeds as follows. To fix ideas assume $k_1\geq 0$ (this can always be done) and $k_2\geq 0$ (the case $k_2\leq 0$ is studied in a similar way). Compute and store the fractional parts of $k_1\nu_1$ for k_1 in some range, and order them in increasing order (keeping track of the corresponding values of k_1). Denote one of these parts as γ_1. Do the same with the fractional parts of $k_2\nu_2$ and denote one of them as γ_2. To have $k_1\nu_1+k_2\nu_2$ very close to an integer one should have $\gamma_1+\gamma_2$ close to one. Scanning the elements γ_1 in increasing order, one should look for the values of γ_2 close to $1-\gamma_1$. As the elements are ordered this scanning takes an effort of the order of a multiple of N, while the effort in the ordering is $O(N\log N)$. This makes the computation feasible even for large values of N.

6 Entropy as a measure of complexity

For many dynamical systems having an important degree of chaoticity, the approach to describe the behaviour of the orbits fails. Despite being deterministic the description is better done by probabilistic methods. So that the relevant objects are now the measures left invariant by the system.

To figure out the degree of complexity of the system one of the most used methods is the (dynamical) entropy. Assume the state space $\mathcal{S}$ compact and consider an invariant measure and normalised in such a way that the total measure is 1 (i.e. we have a probabilistic measure, which will be denoted as μ). Given a finite partition $\mathcal{P}$ of $\mathcal{S}=\cup_{i=1}^{N}P_i$, with all the P_i measurable and satisfying $\mu(P_i\cap P_j)=0$ if $i\neq j$, one can define the entropy of the partition as $h(\mathcal{P})=\sum_{i=1}^{N}(-\mu(P_i)\log(\mu(P_i)))$, as usual. This is a kind of "static" entropy which measures the complexity of the partition, but there is no dynamics on it.

Let us pass to the dynamical aspect. Consider a map T defined in $\mathcal{S}$ and preserving μ. From the partition $\mathcal{P}$ we can compute new partitions, like $T^k(\mathcal{P})$, whose elements are $T^k(P_i),\ i=1,\ldots,N$. Now consider the partition generated by all the sets $T^k(P_i)$ when i ranges from 1 to N and k from 1 to m and denote as h_m the entropy of this partition. Consider $h(\mathcal{P})=\lim_{m\to\infty}h_m/m$. This limit exists for all finite partitions $\mathcal{P}$. The dynamical entropy of the system is defined as the supremum of the values of $h(\mathcal{P})$ when $\mathcal{P}$ ranges over all finite partitions. It is denoted as h or as $h(T)$ if we want to make precise the map that we are using. To make clear that it is an entropy computed from a measure-theoretical point of view, it is customary to call it metric entropy.

The metric entropy of the dynamical system measures the maximal speed of increase of the entropy of the partitions which are generated by the action of the system. With such definition it is clear that it will be possible to compute $h(T)$ (even numerically!) only for simple systems or in a rough way. Fortunately Pesin theory provides a way to obtain the metric entropy from Lyapunov exponents, as we shall see.

6.1 Average on a family of maps

In [15] a rich family of maps is introduced. The state space is the two-dimensional sphere $\mathbb{S}^2$ to be seen as $x^2+y^2+z^2=1$. Let T_ε be a twist around the z-axis. It rotates by $\pi\varepsilon(z+1)$ the points on a given z plane. It is clear that, for any ε, the map T_ε preserves the usual measure μ in $\mathbb{S}^2$. It is assumed that the parameter ε can take any positive value.

Now consider a rotation g in the space (i.e., an element of $SO(3)$). It is identified as a rotation of angle θ around the axis of latitude β and longitude λ (λ is irrelevant). The group $SO(3)$ has an invariant measure, the Haar measure ν, which has a density σ proportional to $\cos(\beta)(1-\cos(\theta))$ (see [15] for a proof). It is also clear that the action of any $g \in SO(3)$, restricted to $\mathbb{S}^2$, preserves μ.

Finally consider

$$F_{\varepsilon,g} = g \circ T_\varepsilon,$$

composition of the two previous maps. Taking into account that g is associated to two angles, θ and β, it is also convenient to consider $F_{\varepsilon,g}$ labelled as $F_{\varepsilon,\theta,\beta}$.

For given $\varepsilon, \theta, \beta$ we can compute the maximal Lyapunov exponent $\ell^1(p)$ for the points p on $\mathbb{S}^2$. The metric entropy $h_{\varepsilon,\theta,\beta}$ of the map $F_{\varepsilon,\theta,\beta}$ is computed by integrating $\ell^1(p)$ with respect to μ:

$$h_{\varepsilon,\theta,\beta} = \int_{\mathbb{S}^2} \ell^1(p) d\mu. \tag{24}$$

For small ε this is a major task due to the wild behaviour of $\ell^1(p)$ with respect to p. It has also a wild dependence with respect to the angles (θ,β). Figure 8 shows the sharp character of $h_{\varepsilon,\theta,\beta} \times \sigma$ with respect to (θ,β) for $\varepsilon = 0.5$ (top right), while for larger ε the behaviour is quite smooth (see Figure 8 top left for $\varepsilon = 3$).

To have an idea of the role of ε, and to obtain a value independent of the concrete rotation g, we can compute an average entropy of the family, for a fixed ε, by integrating with respect to the measure in $SO(3)$

$$\Lambda(\varepsilon) = \int_{SO(3)} h_{\varepsilon,\theta,\beta} d\nu. \tag{25}$$

At the right bottom part of Figure 8 the estimated values of $\Lambda(\varepsilon)$ for small ε are shown. Note that it is a clear indication of behaviour exponentially small with respect to ε. As $\ell^1(p)$ depends strongly on $p \in \mathbb{S}^2$ and then $h_{\varepsilon,\theta,\beta}$ depends also strongly on the two angles, accurate computations of $\Lambda(\varepsilon)$ require a huge amount of estimates of Lyapunov exponents to carry out the integrals in (24) and (25). This has been done for more than hundred values of ε. See [15] for technical details and references.

6.2 The case of randomised maps

On the other hand we can compute the entropy of the "randomised" map. Let us consider a sequence of rotations in $SO(3)$ taken at random with respect to the measure ν: $g_1, g_2, \ldots, g_n, \ldots$. Then, to compute the Lyapunov exponent as in (12), instead of taking the same map at each iteration, we take, successively, the maps $g_n \circ T_\varepsilon$. It is known that independently of the initial point $p \in \mathbb{S}^2$, of the initial vector ξ in the tangent space $T_p\mathbb{S}^2$ and of the selected sequence $\{g_n\}$ in $SO(3)$, the process converges with probability 1 to some value, $R(\varepsilon)$.

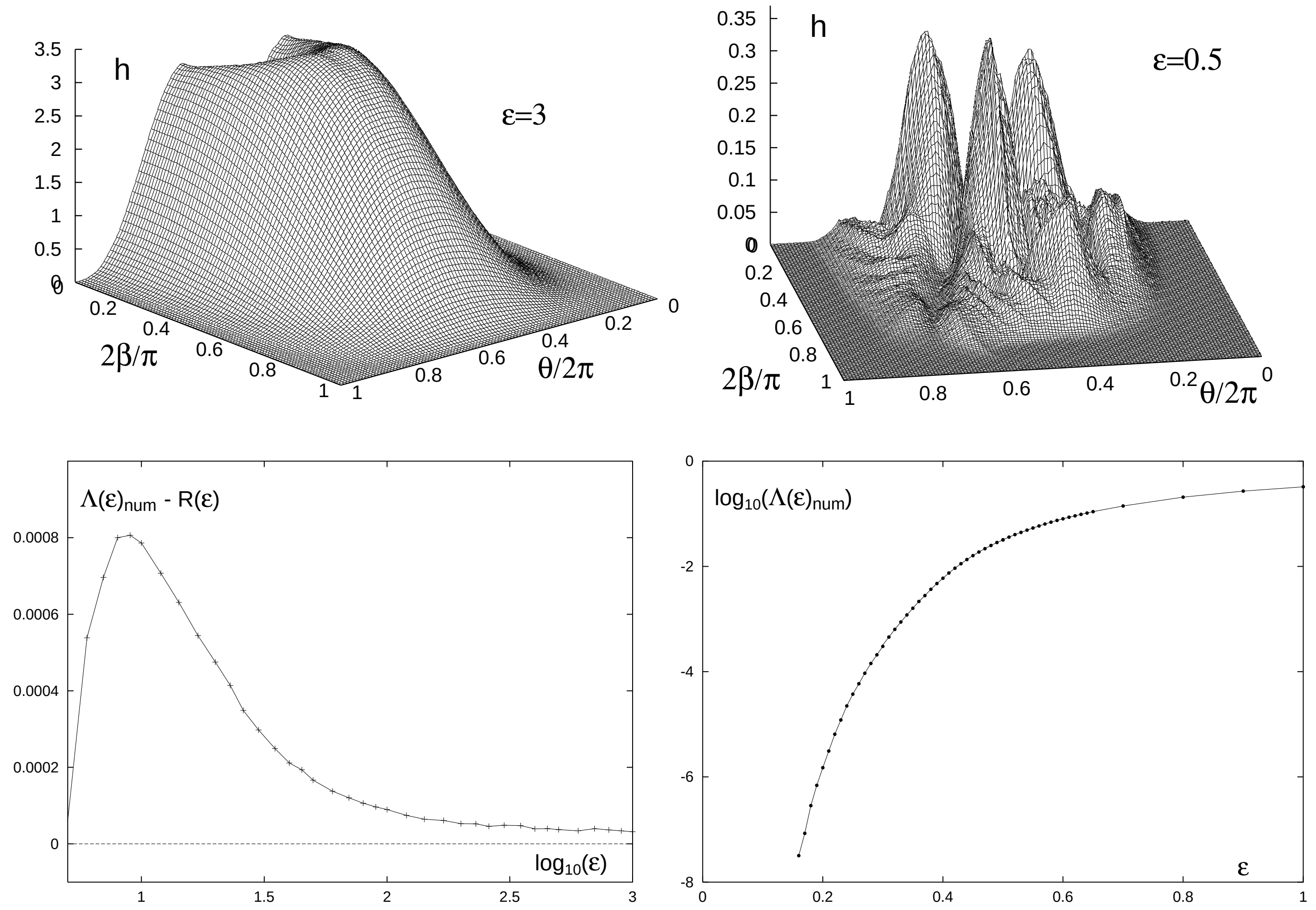

Figure 8: Entropy of a family of area preserving maps in $\mathbb{S}^2$. Top left: The entropy as a function of the latitude of the axis of rotation, β, and the angle of rotation, θ, for a twist parameter $\varepsilon = 3$. Top right: same for $\varepsilon = 0.5$. Bottom left: The difference between the average over $SO(3)$ of the entropy and the entropy of the randomised family, as a function of ε. Bottom right: The average over $SO(3)$ of the entropy for small ε.

In the present case it is even possible to obtain an explicit expression for $R(\varepsilon)$

$$R(\varepsilon) = \int_0^{\frac{1}{2}} \log(1 + (2\pi\varepsilon x(1-x))^2)dx. \tag{26}$$

This integral can be evaluated by numerical quadrature and analytic approximations are easily computed for small and large values of ε.

The plan is to compare the average entropy $\Lambda(\varepsilon)$ with the entropy of the randomised map. Let

$$\Delta(\varepsilon) = \Lambda(\varepsilon) - R(\varepsilon). \tag{27}$$

It is known that for some families of linear maps the inequality $\Delta(\varepsilon) \geq 0$ holds. A natural conjecture is whether this holds for a rich non-linear family as the present one. This would have important consequences. Indeed, it would imply that $h_{\varepsilon,\theta,\beta}$ is positive for a set of rotations of positive measure. Despite the very strong numerical evidence in favour of positiveness, this result has not yet been proved.

From (26) it follows that for small values of ε one has $R(\varepsilon) = \frac{\pi^2}{15}\varepsilon^2 + O(\varepsilon^4)$. On the other hand a rough bound of $\Lambda(\varepsilon)$ gives $\Lambda(\varepsilon) = O(\varepsilon^3)$ (the correct bound seems to be $\Lambda(\varepsilon) \simeq \exp(-\frac{\pi}{\varepsilon})$, but this has not been proved). However even the rough estimate gives $\Delta(\varepsilon) < 0$ for ε small.

For larger ε a plot of $\Delta(\varepsilon)$ is shown in Figure 8 bottom left. Despite this difference is small, the numerical evidence is in favour of $\Delta(\varepsilon) > 0$, even for much larger values of ε than the ones shown in the figure.

7 The role of computers in mathematics

We have seen different examples in dynamical systems where the use of computers has been a key tool to help in clarifying the behaviour of the system. This is common with other domains in mathematics.

Trying to detect places where the use of a computer can help the work of a mathematician, we can consider the following aspects:

- As an experimental tool. Making explorations of the behaviour of a system or, in general, trying to obtain solutions of a system, which symmetries occur in a problem, etc, can help us to "understand" the problem. These explorations can refer to numerical or symbolic aspects. Computers are widely used to manipulate symbols and can encode properties of well-known functions.

- As a method to guess theoretical results. In many of the examples presented here a systematic exploration has allowed to guess a theoretical result.

  It is relatively easy to guess the correct statement of a theorem in easy problems, but one has to be very clever in case of difficult problems. If the problem at hand can be studied numerically or symbolically, this is a valuable tool which cannot be neglected.

  Several examples have been given above where this methodology has been applied. I would like to mention another one which is related to differential equations of Hill's type with quasi-periodic coefficients. Or, equivalently, to 1D Schrödinger equations with quasi-periodic potential. Several interesting properties were discovered numerically in [2]. In particular they give information of the behaviour of the spectrum of Schrödinger operator when the level of energy changes. Later on it has been possible to give complete proofs, see [1], of some of the experimental facts found before. Further work is in progress.

  In general it is very useful, for any problem, to have a priori a good indication on the properties of the solutions.

- To produce rigorous proofs. If the problem has a combinatorial character and one has to analyse a number of cases exceeding manual capabilities, then it is the role of computers to do that task.

  But recent years have seen a flourishing activity in computer-assisted-proofs (CAP). Restricting to dynamical systems, many problems like:

- optimality of estimates in KAM theory (i.e., which is the maximal size of the perturbation such that a torus of given frequencies still exists),
- existence of a strange attractor for Lorenz model and for the numerical values used by Lorenz in his discovery,
- existence of many kinds of choreographies in N-body problems,
- existence of transversal homoclinic and heteroclinic solutions, which implies the existence of many kind of orbits,

just to mention a few ones, have been proved using CAP. The steps in the proofs follow an approach like: a) Prove an abstract theorem in a constructive way and such that all steps can be checkable in the form of inequalities to be satisfied by some computable numbers; b) Use interval arithmetics, which gives rigorous bounds, to check if the required conditions hold.

It is true that in some cases, due to pessimistic estimates of the error, one has to work with many decimal digits. But as the example in Section 4.1 shows, this is no longer a problem (within some limits).

My personal guess is that in a near future the results of careful numerical computations, of moderate complexity, would be turned into rigorous proofs in an almost automatic way.

- Typical statements in analysis contain parts of a sentence like:

$$\ldots \text{ there exists an } \varepsilon_0 > 0 \text{ such that, if } |\varepsilon| < \varepsilon_0, \text{ then } \ldots$$

or

$$\ldots \text{ given } \varepsilon > 0, \text{ there exists a } \delta = \delta(\varepsilon) \text{ such that } \ldots$$

These are existential results. But for applications, and even to understand what goes wrong when the result is not true, it is highly interesting to determine optimal values of ε_0 (such that there are ε with $|\varepsilon| > \varepsilon_0$ for which the result is not true, and to know what happens if $|\varepsilon| = \varepsilon_0$). And to produce constructive ways to obtain explicitly δ as a function of ε. In both types of questions the computers can play a relevant role.

Let us point, finally, that we have considered here deterministic dynamical systems. In a similar way it is possible to study systems with some added noise and stochastic processes. But then the theory is far less well developed. Faced to an experimental phenomenon one can ask how to recognise that it can be modeled by a deterministic system. If the number of available data is large enough there are algorithms to test for determinacy. These algorithms give also an estimate of the minimal dimension in which the system should live. They can require a computational effort ranging from moderate to large.

8 How to face big computational requirements: Super-computing

Last point to consider is the hardware requirements to use the computer as an experimental tool in dynamical systems. It is assumed that to built the software is one of the responsibilities of the researchers. Certainly these values will seem a joke in the near future. Therefore one has to precise that they are given in October 2003.

Scanning some properties in phase and parameter space it seems feasible now to deal with a total of 6 or 7 variables. Of course, one can work with thousands or even millions of variables, but then one is very far from a fairly complete description. Unless the system tends to a very simple dynamics which lives in low dimension.

Just using 100 values for each one of the variables this means that one has to examine some $10^{12} - 10^{14}$ cases, say. Assuming modest requirements for each case, such as $10^4 - 10^6$ elementary operations, we find totals ranging in $10^{16} - 10^{20}$ elementary operations. The largest computer in the world (the NEC Earth Simulator) has a peak performance of $40,960$ GFlop/s. We recall that 1 GFlop/s means 10^9 floating point operations per second. Even running at the peak speed (which is never attainable in realistic problems) this NEC would require 1 month to do 10^{20} Flop.

To satisfy these big computing requirements one uses what is known as supercomputers. A big output can be achieved either with a vectorial structure, which manipulates large vectors working simultaneously with their components, or with a large number of processors, which work in the same or different processes, and with a fast communication between them.

The possibility to assemble a large number of inexpensive processors allows. to many research teams, to do the necessary computations in an autonomous way. This is specially important at the present moment. The last available list of Top 500 (`http://www.top500.org`), dated June 2003, lists only two computers in Spain. None of them devoted to academic/research activities. Last computers in that list have a peak performance of 384 GFlop/s.

Hence, a good solution is to have research teams which become autonomous, building their own supercomputer. The team I am conducting at the University of Barcelona (UB) has one of these machines. Some obsolete nodes are being replaced now, to reach a peak performance of 175 Gflop/s. This means that simulations requiring 10^{16} Flop need roughly one day of CPU time, and large projects up to 10^{18} Flop can need 3 months. The cost of this configuration is around 0.12 Meuro (1 Meuro $= 10^6$ euro).

It is instructive to compare with the past. In 1982 I was director of the Computing Centre at the UB and, after many efforts to convince academic and administrative authorities of this University, we succeeded in replacing a complete obsolete IBM 360/30 by an IBM 4341. The peak performance was 1 MFlop/s, with a cost (at that time) of 1/3 Meuro (which would be not far from 1 Meuro at present). Right now it is possible to have supercomputers with a peak of 1,000 GFlop/s, based on a large set of processors and with fast communications, by the same price. This gives a yearly factor close to 2 in the increase of the performance/price ratio.

One of the standing problems, faced to a huge amount of data, is not to produce them, but how to be able to communicate the results in an understandable way. I am not mentioning the problems of transmission of a large set of data. I mean problems of graphical representation in a large number of variables.

9 Conclusions

The dynamical system theory is a useful tool to understand the structure of many mathematical models of natural sciences, technology and human sciences. They can be used to explain/forecast/control the dynamics.

Numerical and symbolic computations are useful for concrete applications and can be seen as an experimental part of mathematics, even for theoretical purposes. One can suggest the correct results, automatise parts of some proofs and, in general, to understand the system even if a full theoretical study is out of reach.

The necessary resources are now widely available at a reasonable cost.

Acknowledgements

Support by grants DGICYT BFM2000-805 (Spain), CIRIT 2001 SGR-70 (Catalonia) and partial support of grant INTAS 2000-221 is acknowledged.

References

[1] Broer, H. W., Puig, J., Simó, C.: Resonance tongues and instability pockets in the quasi–periodic Hill–Schrödinger equation, *Comm. in Mathematical Physics*, **241** (2003), 467–503.

[2] Broer, H. W., Simó, C.: Hill's equation with quasi-periodic forcing: resonance tongues, instability pockets and global phenomena. *Bul. Soc. Bras. Mat.* **29** (1998), 253–293.

[3] Broer, H. W., Simó, C., Tatjer, J. C.: Towards global models near homoclinic tangencies of dissipative diffeomorphisms, *Nonlinearity*, **11** (1998), 667–770.

[4] Broer, H. W., Simó, C., Vitolo, R.: Bifurcations and strange attractors in the Lorenz-84 climate model with seasonal forcing. *Nonlinearity* **15** (2002) 1205–1267.

[5] Broer, H. W., Simó, C., Vitolo, R.: The Hopf-saddle-node bifurcation for fixed points of diffeomorphisms. In progress.

[6] Chenciner, A., Gerver, J., Montgomery, R., Simó, C.: Simple Choreographic Motions of N Bodies: A Preliminary Study. In *Geometry, Mechanics and Dynamics*, ed. P. Newton, P. Holmes, A. Weinstein, pp. 287–308, Springer-Verlag, 2002.

[7] Chenciner, A., Montgomery, R.: A remarkable periodic solution of the three body problem in the case of equal masses. *Annals of Math.* **152** (2000), 881–901.

[8] Cincotta, P. M., Giordano, C. M., Simó, C.: *Physica D* **182** 151–178 (2003).

[9] Cincotta, P. M., Simó, C.: Simple tools to study global dynamics in non–axisymmetric galactic potentials – I. *Astronomy & Astrophysics Supp.* **147** (2000), 205–228.

[10] Dumortier, F., Ibáñez, S., Kokubu, H., Simó, C.: Homoclinic and heteroclinic cycles in the unfolding of the Hopf-Zero singularity for 3D vector fields. In progress.

[11] Gómez, G., Jorba, À., Masdemont, J., Simó, C.: *Dynamics and Mission Design Near Libration Points. Volumes 3 & 4*, World Sci. Pub., Monograph Ser. Math., Singapore, xiv+187 pp. & xii+262 pp., 2000.

[12] Gómez, G., Llibre, J., Martínez, R., Simó, C.: *Dynamics and Mission Design Near Libration Points. Volumes 1 & 2*, World Sci. Pub., Monograph Ser. Math., Singapore, xx+442 pp. & xii+146 pp., 2001.

[13] Gómez, G., Mondelo, J. M., Simó, C.: Refined Fourier analysis: procedures, error estimates and applications. Preprint 2001. Available at `http://www.maia.ub.es/dsg`.

[14] Grau, M., Simó, C.: Invariant manifolds in Sitnikov problem. In progress.

[15] Ledrappier, F., Shub, M., Simó, C., Wilkinson, A.: Random versus deterministic exponents in a rich family of diffeomorphisms, *J. Stat. Phys.*, **113** (2003), 85–149.

[16] Martínez, R., Simó, C.: Simultaneous binary collisions in the planar four body problem, *Nonlinearity* **12** (1999), 1–28.

[17] Martínez, R., Simó, C.: The degree of differentiability of the regularization of simultaneous binary collisions in some N–body problems. *Nonlinearity* **13** (2000), 1–24.

[18] Martínez, R., Simó, C., Suín, A.: Regularizable and non-regularizable collisions in N-body problems. Proceedings EQUADIFF 99, Berlin, ed. B. Fiedler, K. Gröger y J. Sprekels, 12-19, World Scientific, Singapore 2000.

[19] Martínez, R., Simó, C.: Relative equilibrium solutions of the Newtonian five-body problem. In progress.

[20] McGehee, R.: A stable manifold theorem for degenerate fixed points with applications to celestial mechanics. *J. of Diff. Equations* **14** (1973), 70–88.

[21] Moser, J.: "Stable and Random Motions in Dynamical Systems", Annals of Mathematics Studies, Princeton Univ. Press, 1973.

[22] Simó, C.: Relative equilibrium solutions in the four-body problem. *Celestial Mechanics*, **18** (1978), 165–184.

[23] Simó, C.: Analytical and numerical computation of invariant manifolds, in D. Benest and C. Froeschlé, ed.: "Modern Methods in Celestial Mechanics", Editions Frontières, Paris (1990), 285–330.

[24] Simó, C.: Averaging under fast quasi-periodic forcing, in J. Seimenis, ed.: "Hamiltonian mechanics: Integrability and Chaotic Behaviour", *NATO-ASI Series B: Physics.* Plenum, New York (1994) pp. 13–34.

[25] Simó, C.: Splitting and arithmetics. Lecture given at the EQUADIFF 95 Conference, Lisboa (1995), unpublished.

[26] Simó, C.: Effective Computations in Celestial Mechanics and Astrodynamics, in V. V. Rumyantsev and A. V. Karapetyan, ed.: "Modern Methods of Analytical Mechanics and their Applications" *CISM Courses and Lectures* **387** Springer, Heidelberg (1998) pp. 55–102.

[27] Simó, C.: New families of Solutions in N–Body Problems, in C. Casacuberta et al., ed.: "Proceed. 3rd European Cong. of Math." *Progress in Math.* **201**, Birkäuser, Basel (2001) pp. 101–115.

[28] Simó, C.: Global Dynamics and Fast Indicators, in H. W. Broer et al., ed.: "Global Analysis of Dynamical Systems", IOP Publishing, Bristol (2001) pp. 373–390.

[29] Simó, C.: Dynamical properties of the figure eight solution of the three-body problem. In A. Chenciner et al., ed.: "Proceed. Celestial Mechanics Conference", Evanston, 1999, *Contemporary Mathematics, AMS* **292** (2000) pp. 209–228.

[30] Simó, C., Stuchi, T.: Central Stable/Unstable Manifolds and the destruction of KAM tori in the planar Hill problem. *Physica D* **140** (2000), 1–32.

[31] Simó, C., Valls, C.: A formal approximation of the splitting of separatrices in the classical Arnold's example of diffusion with two equal parameters. *Nonlinearity* **14** (2001), 1707–1760.